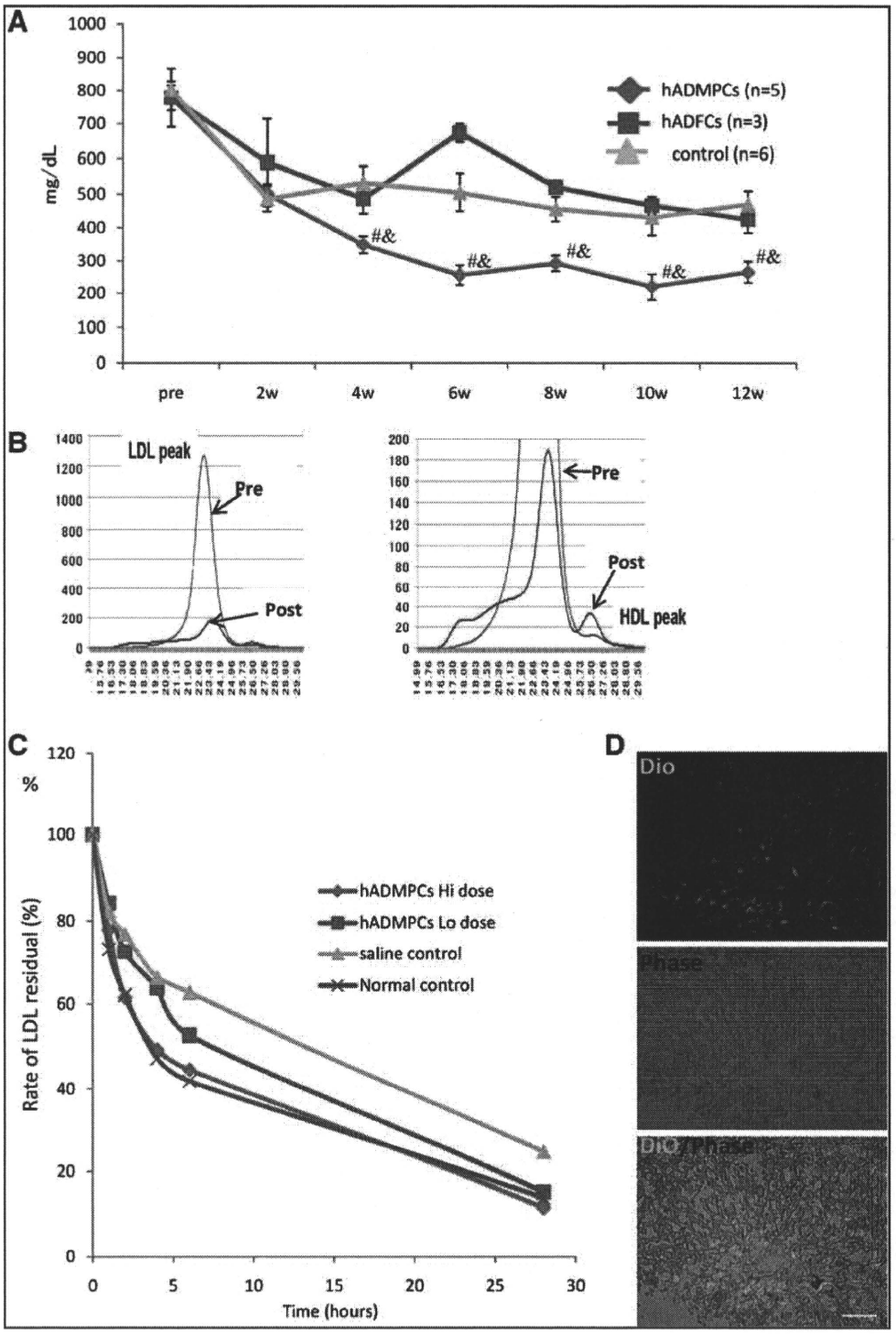

FIG. 3. **(A)** Total serum cholesterol levels. hADMPC transplantation in WHHL rabbits was followed for 12 weeks. Total serum cholesterol was measured in five rabbits that each received 3×10^7 hADMPCs, three rabbits that each received 3×10^7 hADFCs, and in six rabbits that received saline (control). Bars indicated mean ± standard error of the mean (SEM) ($^{\#}p < 0.05$; control vs. the hADMPC-transplanted WHHL rabbit; $^{\&}p < 0.05$; the hADFC-transplanted WHHL rabbit vs. the hADMPC-transplanted WHHL rabbit). **(B)** Lipoprotein profiles in a representative WHHL rabbit with hADMPC transplantation after gel filtration. Serum samples from the WHHL rabbit before and 4 weeks after transplantation were fractionated. Note the marked reduction in low-density lipoprotein (LDL) peak and appearance of high-density lipoprotein (HDL) peak. **(C)** Rate of clearance of LDL from the serum of rabbits with and without transplantation of hADMPCs. Animals were injected with ^{125}I-labeled human LDL, and the time course of clearance was monitored following trichroloacetic acid precipitation of serum at time 5 min, 1 h, 2 h, 4 h, 6 h, and 28 h. Residual ^{125}I-LDL was expressed as percentages of that at 5 min. $^{\#}p < 0.05$ (control vs. the hADMPC-transplanted WHHL rabbit [low dose]) and $^{*}p < 0.05$ (control vs. the hADMPC-transplanted WHHL rabbit [high dose]). **(D)** DiO-LDL uptake into hADMPC-derived hepatocytes in the WHHL rabbi liver. Thin-sliced recipient liver was incubated with DiO-labeled LDL in the serum-free medium for 24 h. After washing and fixation, the incubated slices were applied for fluorescent microscopy. DiO-LDL uptake cells (green) and no uptake parenchymal cells were observed in the section. Bar = 100 μm.

drogenase expression. To confirm that hADMPCs differentiated into hepatocytes *in vivo*, the cells before transplantation and human primary hepatocytes (Invitrogen, Lot number; HuP81) were applied for quantitative PCR as control.

Clearance of ^{125}I-LDL from rabbit serum

WHHL rabbits (8 weeks old) were anesthetized with pentobarbital (50 mg/kg). The peritoneum was incised and hADMPCs (high-dose; 3×10^7 cells/rabbit, $n=2$, low-dose; 5×10^6 cells/rabbit, $n=2$) suspended in 3 mL of HBSS (20°C) ($n=5$) or 3 mL of control saline ($n=2$) were infused into the portal vein via a 18-gauge Angiocath (BD). The rabbits were immunosuppressed using the protocol illustrated in Figure 1A. Eight weeks later, the animals were tested by the LDL turnover assay. ^{125}I human LDL (BT-913R, Lot No. 9130709; Biomedical Technologies Inc.) was delivered via the marginal ear vein of the WHHL rabbits and normal control

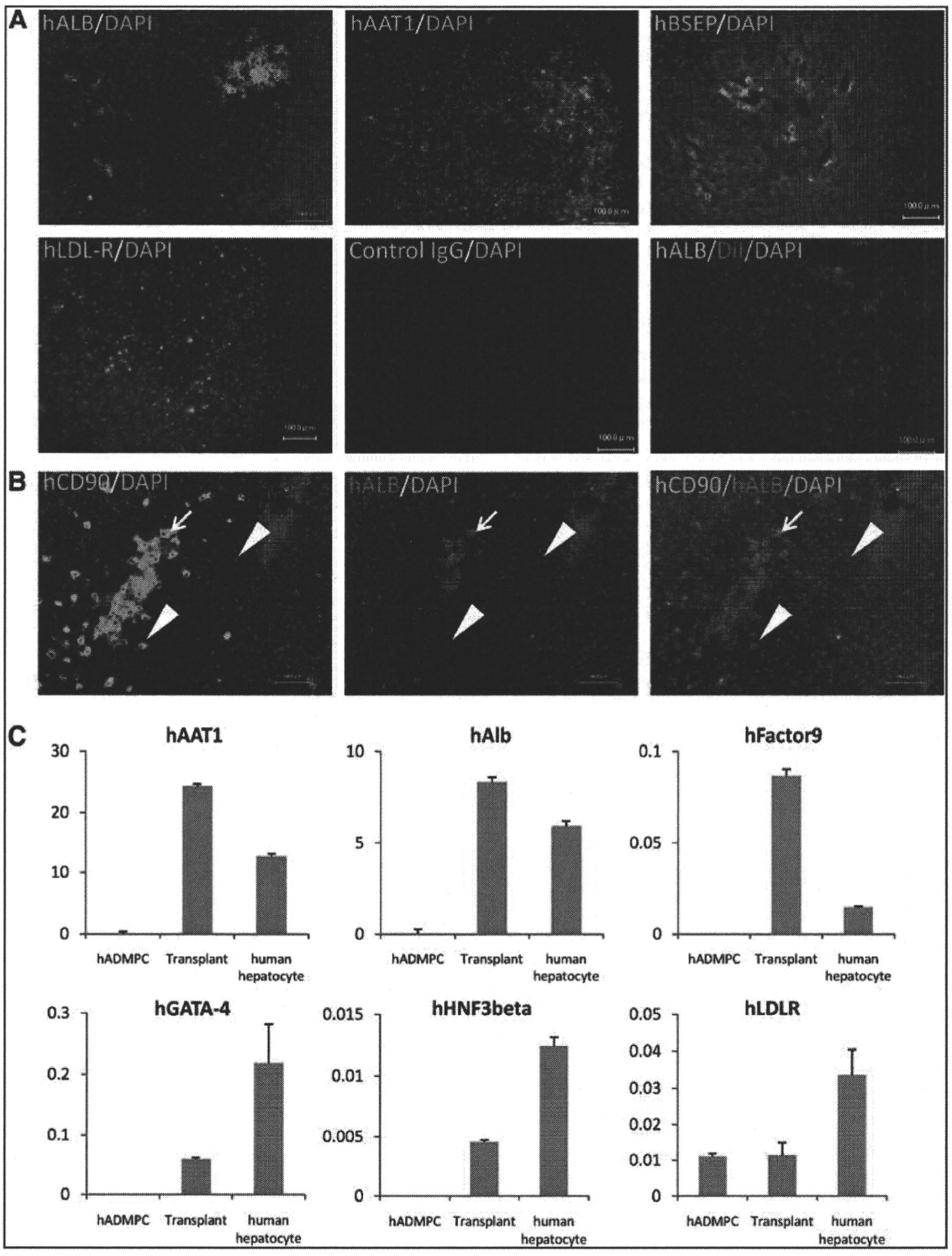

rabbits in physiological saline containing 2 mg/mL bovine serum albumin. Blood was collected from the opposite ear after injection at 5 min, 1 h, 2 h, 4 h, 6 h, and 28 h. ^{125}I-labeled apolipoprotein B-containing LDL was precipitated with 20% of trichloroacetic acid (Wako Pure Chemical Industries) (serum; 320 μL, 100% w/v trichloroacetic acid (TCA) 80 μL), and then the precipitants were applied for counting.

Uptake of DiO-labeled LDL by transplants ex vivo

Human LDL (1.019–1.063 g/mL) was isolated by sequential ultracentrifugation from normolipidemic donors as previously described,[24] dialyzed against saline-EDTA, and then sterilized by filtration through a 0.2 μm filter. Lipoproteins were labeled with 3,3′-dioctadecyloxacarbocyanine perchlorate (DiO; Sigma) by incubating the LDL in 0.5% bovine serum albumin/PBS with 100 mL DiO in dimethyl sulfoxide (3 mg/mL) for 8 h at 37°C. The lipoproteins were obtained by sequential ultra centrifugation (1.019–1.063 g/mL) as described,[14] and then dialyzed against PBS and filtered before use. To evaluate the uptake of DiO-LDL by transplants *ex vivo*, thin-sliced WHHL rabbit liver tissue were incubated with serum-free Dulbecco's modified Eagle's medium containing 10 μg/mL DiO-LDL for 24 h at 37°C. Finally, the incubated slices were rinsed, fixed with 10% formalin, sectioned into 5 μm thickness, and mounted with Perma-Flour (Japan Tanner Corporation). The slides were examined using a BioZero laser scanning microscope (Kyence).

Statistical analysis

Values were expressed as mean ± standard error of the mean. Differences between mean values of treated and untreated groups were evaluated using the Student's *t*-test. A p-value < 0.05 was considered statistically significant. All statistical analyses were performed using the SPSS Statistics 17.0 package (SPSS Inc.).

Results

Characteristics of hADMPCs

The cells obtained from adipose tissue were seeded and incubated for 24 h (Fig. 1Ai). After incubation, the adherent cells were treated with EDTA solution, and the resulting suspended cells were replated at a density of 10,000 cells/cm^2 on human fibronectin-coated dishes (BD BioCoat) (Fig. 1Aii and 1Aiii). Within two to three passages after the initial plating of the primary culture, hADMPCs appeared as a monolayer of large flat cells (25–30 μm in diameter). As the cells approached confluence, they assumed a more spindle-shaped, fibroblastic morphology (Fig. 1Aiv). After passaging five to six times, the hADMPCs were applied for transplantation. We used flow cytometry to assess markers expressed by hADMPCs (Fig. 1B). The cells were negative for markers of the hematopoietic lineage (CD45) and of hematopoietic stem cells, ABCG-2, CD34, and CD133. They were also negative for CD31, an endothelial cell-associated marker and the surface antigen c-Kit (CD117). However, they stained positively for a number of surface markers characteristic of mesenchymal and/or neural stem cells, but not embryonic stem cells, including CD29, CD44 (hyaluronan receptor), CD73, CD105 (endoglin), and CD166. hADMPCs also were positive for stage-specific embryonic antigen-4. Next, adipogenic, osteogenic, and chondrogenic differentiation potential of hADMPCs were examined (Fig. 1C). Adipogenic differentiation was induced by culture with differentiation medium containing 1-methyl-3-isobutylxanthine (a peroxisome proliferator-activated receptor γ agonist), dexamethasone, and insulin. Induction was confirmed by the accumulation of intracellular lipid droplets that were stained with Oil Red O. After 7-day induction for osteogenesis, hADMPCs were stained with Alizarin red S for mineralized nodules. hADMPCs showed intense Alcian Blue staining, indicating chondrogenic induction capability of hADMPCs.

Serum cholesterol in WHHL rabbit with transplants

hADMPCs were separated from human subcutaneous adipose tissues, cultured for five to seven passages, and applied for transplantation into WHHL rabbits. WHHL rabbits received immunosuppressants and an antiviral agent as illustrated in Figure 2A, and then were transplanted 3×10^7 hADMPCs by portal vein infusion (Fig. 2B). At the day of and 1, 2, 4, 6, and 10 weeks after transplantation of hADMPCs via the portal vein, we examined whether the cells reside or not in the liver after transplantation. Typical

FIG. 4. **(A)** Immunohistochemical identification of human hepatocytic marker cells in liver sections of WHHL rabbits after hADMPC transplantation. Twelve weeks after hADMPC transplantation, human albumin-, human alpha-1-antitrypsin-, human bile salt export pump (BSEP)-, and LDL-receptor-positive cells were dispersed within the perivenous regions of the liver parenchyma, where they made contact with and integrated among the host cells with cell–cell interactions between hADMPC-derived cells and diseased hepatocytes pair. Ten weeks after transplantation of DiI-stained hADMPCs, copresence of human albumin (green) and pretreated DiI-fluorescence (red) on the same cells was observed. Bar = 100 μm. **(B)** Differentiation of transplanted hADMPCs into hepatocyte-like cells. Twelve weeks after transplantation, almost but not all human CD90-positive cells expressed human albumin, indicating that major population of transplanted hADMPCs could differentiate into hepatocyte-like cells (left panel: human CD90; middle panel: human albumin; right panel: merge). Arrows indicate human CD90 and human albumin double-positive cells; arrowheads indicate human CD90-positive but human albumin-negative cells. **(C)** Human hepatic gene expression in WHHL rabbit liver after hADMPC transplantation. RNA was prepared from the WHHL rabbit liver 12 weeks after hADMPC transplantation. We used the following hepatic markers: human alpha-1-antitrypsin, human albumin, human factor IX, human GATA-binding protein 4 (GATA-4), human hepatocyte nuclear factor 3 (HNF-3) beta, and human LDL-receptor. Their expression levels were examined by quantitative real time-polymerase chain reaction (RT-PCR) using Assays-on-Demand Gene Expression Assay Mix. The livers of WHHL rabbits that received saline ($n = 3$) were negative for human hepatic genes. The mRNA levels were normalized based on human glyceraldehyde-3-phosphate dehydrogenase expression as housekeeping gene and data are mean ± SEM of triplicate experiments. The livers of WHHL rabbits that received hADMPC transplantation ($n = 3$) were positive for human hepatic genes, and their expression levels were similar to those of human primary hepatocytes but not hADMPCs *per se*. Data are mean ± SEM.

distribution patterns of transplanted hADMPCs were followed in Figure 2C. DiI-fluorescent labeled-hADMPCs resided and distributed in the portal area at the day of transplantation. Six and 10 weeks after transplantation, DiI-positive transplanted cells migrated into centrilobular direction. Next, to demonstrate certain percentage of repopulation of the transplanted cells in the liver, the ratios of human-derived cell repopulation were examined by analyzing a repetitive DNA sequence at the day of and 2, 4, 6, and 12 weeks after transplantation (Fig. 2D). To indicate standard curve, we mixed the indicated percentage of hADMPCs with rabbit hepatocytes and plotted the obtained the amount of *Alu* PCR products, and estimated the amount of repopulation of the transplanted cells in the liver. At the day of transplantation, the ratio of hADMPCs to whole WHHL rabbit liver cells was $0.21\% \pm 0.056\%$ (mean $\pm$ standard error of the mean) and the ratio decreased to $0.016\% \pm 0.002\%$, $0.011\% \pm 0.001\%$, and $0.009\% \pm 0.0001\%$ after 2, 4, and 8 weeks of transplantation, respectively. After 12 weeks of transplantation, the ratio was increased to $0.024\% \pm 0.00005\%$ as indicated (Fig. 2D).

To reveal the effects of hADMPC transplantation onto the lipid profiles of the WHHL rabbit, serum cholesterol levels were monitored over 12 weeks (Fig. 3A). Significant reductions in total serum cholesterol were observed within 4 weeks of the transplantation, and the reductions were maintained for the entire period. The reduction in serum cholesterol in the animals that received hADMPC transplantation was significantly greater than that of the control group. To determine the effects of hADMPC transplantation on the fractions of high-density lipoprotein and LDL in recipient animals, fractionation by fast protein liquid chromatography was performed (Fig. 3B). Transplantation of hADMPCs resulted in marked reduction of the peak LDL-cholesterol and increment of high-density lipoprotein cholesterol fraction (right panel).

Next, clearance experiments were performed with human LDL to confirm that the transplanted hADMPCs contributed the fall in serum cholesterol through uptake of LDL via LDL receptors. The rate of LDL clearance was significantly higher in the WHHL rabbits with transplanted hADMPCs than WHHL rabbits without transplanted hADMPCs (Fig. 3C). Rabbits with hADMPC transplants showed ~2.4-fold (high-dose; 3×10^7 cells/rabbit) and 1.4-fold (low-dose; 5×10^6 cells/rabbit) increase in the rate of LDL cholesterol clearance.

To evaluate the uptake of DiO-LDL by transplants *ex vivo*, thin-sliced WHHL rabbit liver was incubated with DiO-labeled LDL for 24 h and the uptake was examined as clearance experiment (Fig. 3D). DiO-LDL was uptaken by some but not all of the cells in the WHHL rabbit liver transplanted with hADMPCs. The DiO-LDL-uptaking cells were seen dispersed, contacted, and integrated among the nonuptaking parenchymal cells, suggesting that hADMPCs differentiated into hepatocytes *in vivo*, lowered of serum cholesterol via LDL uptake.

hADMPCs reside, survive, and differentiate into hepatocytes in vivo

After establishment of the graft as indicated by long-term lowering of serum cholesterol, human-specific hepatocytic proteins, such as albumin, alpha-1-antitrypsin, bile salt export pump, and LDL-receptor, positive cells were identified dispersed within perivenous regions of the liver parenchyma, where they have contacted and integrated among the host cells (Fig. 4A), with cell–cell interactions conserved between hADMPC-derived hepatocytes and diseased hepatocytes pair. Ten weeks after transplantation of DiI-prestained hADMPCs, copresence of human albumin (green) and pretreated DiI-fluorescence (red) on the same cells was observed (Fig. 4A), indicating the transplanted hADMPCs might differentiate into hepatocyte-like cells. To confirm transplanted hADMPCs might differentiate into hepatocyte-like cells and to reveal the efficacy of differentiation, the colocalization of human CD90 and human albumin was examined. As shown in Figure 4B, almost but not all human CD90-positive cells expressed human albumin, indicating that about 80% or more of transplanted hADMPCs could differentiated into human albumin-positive hepatocyte-like cells 12 weeks after transplantation. Next, to confirm the differentiation of hADMPCs into hepatocytes *in vivo*, expression of hepatocyte markers was analyzed by quantitative RT-PCR. The WHHL rabbit liver that was transplanted with hADMPCs expressed higher levels of human-specific alpha-1-antitrypsin, albumin, and coagulation factor IX than hADMPCs (Fig. 4C). The expression levels of human GATA-4, human hepatocyte nuclear factor 3 beta, and LDL-receptor were also higher in the WHHL rabbit liver than hADMPCs (Fig. 4C). These results indicate that hADMPCs differentiate into mature hepatocytes *in vivo*.

Discussion

We have used the WHHL rabbit to study the ability of hADMPC-derived hepatocytes to lower serum cholesterol in an animal model of FH. Our results have shown that hADMPCs transplanted into the rabbit liver differentiate into hepatocytes *in vivo* and effectively clear LDL from the circulation.

The reductions in cholesterol brought about by the engrafted hADMPC-derived hepatocytes suggest that human LDL receptors can act as replacement for the mutant LDL receptors in the WHHL rabbit. This capacity of hADMPC-derive hepatocytes is not unexpected, as the liver is the most important site of LDL uptake, accounting for >50% of total removal from the circulation, and the liver is only organ capable of converting cholesterol to bile for excretion. The substantial decrease in serum cholesterol achieved suggests that the hADMPC-derived hepatocytes both internalize LDL and metabolize the cholesterol to bile for excretion. The correlation between cholesterol and coronary heart disease has been well documented, and decreases in serum cholesterol of the magnitude that we have demonstrated would be expected to decrease morbidity and mortality in the patients with severe FH.[25]

The appearance of the hADMPC-derived hepatocytes as revealed by immunohistochemistry and RT-PCR indicated that the hADMPCs differentiated into hepatocytes and integrated into the liver parenchyma. The perivenous migration of the differentiated hepatocytes derived from hADMPCs along the portal-venous axis and suggests that hADMPCs recognize conserved signals on host cells and matrix. There are some reports describing the hepatogenic differentiation potential of hADMPCs.[15,16] These studies

described that hepatocytes differentiated from hADMPCs *ex vivo* engrafted in the liver and functioned, and that the hADMPCs could be resided and changed their characters into hepatocyte-like cells only in the chemically damaged liver. These reports, revealing that hADMPCs have capabilities to differentiate into hepatocytes, hinted us that hADMPCs might differentiate into hepatocytes in liver. Hepatogenic signals from the microenvironment such as cell-to-cell connections or intermediates are probably important factors that dictate the type of functional hepatocytes in hepatic differentiation.[26] We are currently investigating the mechanism for the differentiation hADMPCs into hepatocytes.

The choice of cell source is critical for realizing success in cellular therapy. Liposuction surgeries yield a massive amount of lipoaspirate adipose tissue from 100 mL to >3 L as cell sources.[27] A major advantage of hADMPCs is their availability in safe and easy with few ethical issues, as compared with the shortage of human livers for orthotopic transplantation, which has been shown to be effective for the treatment of FH.[25] Our serum cholesterol reduction studies and *in vitro* studies demonstrated that human LDL binds to the hADMPC-derived hepatocytes receptor, indicating that this therapy will be useful in humans. Previous attempts to study the efficacy of hepatocyte transplantation in the WHHL rabbit model have employed allogenic hepatocytes, xenogenic hepatocytes, or hepatocytes transduced *ex vivo* with a recombinant retrovirus containing the LDL receptor cDNA.[6–13] The lowering effects of hepatocyte transplantation on serum cholesterol have been reported, but there was some problems. First, hepatocytes could not be expanded *ex vivo* with functional potentials; second, the cell viability reduced after cryopreservation; third, the many injected hepatocytes are supposed to be cleared by the reticuloendothelial system or lose viability during early phase. The rate of LDL clearance was returned to normal in LDL receptor knockout mice by introduction of an adenoviral construct containing an LDL receptor cDNA, and similar approaches have lowered serum cholesterol levels in the WHHL rabbit.[10,12,13] However, sustained expression of the LDL receptor from viral vectors can be difficult to achieve.[11,13] Moreover, hepatocytes derived from hADMPCs have the advantage that the LDL receptor is expressed from an endogenous gene with intact regulatory sequences. Such control of LDL receptor levels would not be expected after treatment of hypercholesterolemia with LDL receptor cDNA construct that lack the regulatory regions of the gene.[28]

Our experiments have shown that the hADMPCs expressed hepatocyte markers after transplantation *in vivo* and the integrated cells into parenchyma provide functional LDL receptors, indicating that they differentiated into hepatocytes and might lower serum cholesterol in the WHHL rabbit. These results suggested that hADMPC transplantation via portal vein could correct the metabolic defects of FH patients and that hADMPC-derived hepatocytes could function as supplier with plasma proteins derived from liver, giving us an idea that hADMPC-transplantation might be a novel cell therapy for hemophilia, alpha-1 antitrypsin deficiency, mucolipidosis, and other diseases caused by genetic defects for liver function. In near future, the therapy will be a novel therapy for kinds of inherited liver diseases.

Acknowledgments

This study was supported in part by the Program for Promotion of Fundamental Studies in Health Sciences of the National Institute of Biomedical Innovation (NIBIO), RIKEN Program for Drug Discovery and Medical Technology Platforms, and Kobe Translational Research Cluster, the Knowledge Cluster Initiative, Ministry of Education, Culture, Sports, Science and Technology (MEXT).

Disclosure Statement

All of the authors stated no conflict of interest.

References

1. Brown, M.S., and Goldstein, J.L. A receptor-mediated pathway for cholesterol homeostasis. Science **232,** 34, 1986.
2. Havel, R.J., Yamada, N., and Shames, D.M. Watanabe heritable hyperlipidemic rabbit. Animal model for familial hypercholesterolemia. Arteriosclerosis **9(1 Suppl),** I33, 1989.
3. Yamamoto, T., Bishop, R.W., Brown, M.S., Goldstein, J.L., and Russell, D.W. Deletion in cysteine-rich region of LDL receptor impedes transport to cell surface in WHHL rabbit. Science **32,** 1230, 1986.
4. Bujo, H., Takahashi, K., Saito, Y., Maruyama, T., Yamashita, S., Matsuzawa, Y., Ishibashi, S., Shionoiri, F., Yamada, N., and Kita, T. Clinical features of familial hypercholesterolemia in Japan in a database from 1996–1998 by the research committee of the ministry of health, labour and welfare of Japan. J Atheroscler Thromb **11,** 146, 2004.
5. Yamashita, S., Hbujo, H., Arai, H., Harada-Shiba, M., Matsui, S., Fukushima, M., Saito, Y., Kita, T., and Matsuzawa, Y. Long-term probucol treatment prevents secondary cardiovascular events: a cohort study of patients with heterozygous familial hypercholesterolemia in Japan. J Atheroscler Thromb **15,** 292, 2008.
6. Gunsalus, J.R., Brady, D.A., Coulter, S.M., Gray, B.M., and Edge, A.S. Reduction of serum cholesterol in Watanabe rabbits by xenogeneic hepatocellular transplantation. Nat Med **3,** 48, 1997.
7. Tejera, M.L., Cienfuegos, J.A., Maganto, P., Pardo, F., Santamaria, L., Codesal, J., De Andres, S., Hernandez, J.L., and Castillo-Olivares, J.L. Reduction of cholesterol levels following liver cell grafting in hyperlipidemic (WHHL) rabbits. Transplant Proc **24,** 160, 1992.
8. Wang, J., Pollak, R., and Bartholomew, A. Sustained reduction of serum cholesterol levels following allo-transplantation of parenchymal hepatocytes in Watanabe rabbits. Transplant Proc **23,** 894, 1991.
9. Wiederkehr, J.C., Kondos, G.T., and Pollak, R. Hepatocyte transplantation for the low-density lipoprotein receptor-deficient state. A study in the Watanabe rabbit. Transplantation **50,** 466, 1990.
10. Chowdhury, J.R., Grossman, M., Gupta, S., Chowdhury, N.R., Baker, J.R., Jr., and Wilson, J.M. Long-term improvement of hypercholesterolemia after *ex vivo* gene therapy in LDLR-deficient rabbits. Science **254,** 1802, 1991.
11. Ishibashi, S., Brown, M.S., Goldstein, J.L., Gerard, R.D., Hammer, R.E., and Herz, J. Hypercholesterolemia in low density lipoprotein receptor knockout mice and its reversal by adenovirus-mediated gene delivery. J Clin Invest **92,** 883, 1993.
12. Kozarsky, K.F., McKinley, D.R., Austin, L.L., Raper, S.E., Stratford-Perricaudet, L.D., and Wilson, J.M. *In vivo* correction

of low density lipoprotein receptor deficiency in the Watanabe heritable hyperlipidemic rabbit with recombinant adenoviruses. J Biol Chem **269,** 13695, 1994.
13. Wilson, J.M., Chowdhury, N.R., Grossman, M., Wajsman, R., Epstein, A., Mulligan, R.C., and Chowdhury, J.R. Temporary amelioration of hyperlipidemia in low density lipoprotein receptor-deficient rabbits transplanted with genetically modified hepatocytes. Proc Natl Acad Sci U S A **87,** 8437, 1990.
14. Okura, H., Komoda, H., Saga, A., Kakuta-Yamamoto, A., Hamada, Y., Fumimoto, Y., Lee, C.M., Ichinose, A., Sawa, Y., and Matsuyama, A. Properties of hepatocyte-like cell clusters from human adipose tissue-derived mesenchymal stem cells. Tissue Eng Part C Methods **16,** 761, 2010.
15. Banas, A., Teratani, T., Yamamoto, Y., Tokuhara, M., Takeshita, F., Quinn, G., Okochi, H., and Ochiya, T. Adipose tissue-derived mesenchymal stem cells as a source of human hepatocytes. Hepatology **46,** 219, 2007.
16. Seo, M.J., Suh, S.Y., Bae, Y.C., and Jung, J.S. Differentiation of human adipose stromal cells into hepatic lineage *in vitro* and *in vivo*. Biochem Biophys Res Commun **328,** 258, 2005.
17. Komoda, H., Okura, H., Lee, C.M., Sougawa, N., Iwayama, T., Hashikawa, T., Saga, A., Yamamoto, A., Ichinose, A., Murakami, S., Sawa, Y., and Matsuyama, A. Reduction of N-glycolylneuraminic acid xenoantigen on human adipose tissue-derived stromal cells/mesenchymal stem cells leads to safer and more useful cell sources for various stem cell therapies. Tissue Eng Part A **16,** 1143, 2010.
18. Okura, H., Matsuyama, A., Lee, C.M., Saga, A., Kakuta-Yamamoto, A., Nagao, A., Sougawa, N., Sekiya, N., Takekita, K., Shudo, Y., Miyagawa, S., Komoda, H., Okano, T., and Sawa, Y. Cardiomyoblast-like cells differentiated from human adipose tissue-derived mesenchymal stem cells improve left ventricular dysfunction and survival in a rat myocardial infarction model. Tissue Eng Part C Methods **16,** 417, 2010.
19. Bjorntorp, P., Karlsson, M., Pertoft, H., Pettersson, P., Sjostrom, L., and Smith, U. Isolation and characterization of cells from rat adipose tissue developing into adipocytes. J Lipid Res **19,** 316, 1978.
20. Zuk, P.A., Zhu, M., Ashjian, P., De Ugarte, D.A., Huang, J.I., Mizuno, H., Alfonso, Z.C., Fraser, J.K., Benhaim, P., and Hedrick, M.H. Human adipose tissue is a source of multipotent stem cells. Mol Biol Cell **13,** 4279, 2002.
21. Nicklas, J.A., and Buel, E. Development of an Alu-based, real-time PCR method for quantitation of human DNA in forensic samples. J Forensic Sci **48,** 936, 2003.
22. Opel, K.L., Fleishaker, E.L., Nicklas, J.A., Buel, E., and McCord, B.R. Evaluation and quantification of nuclear DNA from human telogen hairs. J Forensic Sci **53,** 853, 2008.
23. Okazaki, M., Usui, S., Ishigami, M., Sakai, N., Nakamura, T., Matsuzawa, Y., and Yamashita, S. Identification of unique lipoprotein subclasses for visceral obesity by component analysis of cholesterol profile in high-performance liquid chromatography. Arterioscler Thromb Vasc Biol **25,** 578, 2005.
24. Bier, D.M., and Havel, R.J. Activation of lipoprotein lipase by lipoprotein fractions of human serum. J Lipid Res **11,** 565, 1970.
25. Steinberg, D., and Witztum, J.L. Current concepts. Lipoproteins and atherogenesis. Current concepts. JAMA **264,** 3047, 1990.
26. Hughes, R.D., Mitry, R.R., and Dhawan, A. Hepatocyte transplantation for metabolic liver disease: UK experience. J R Soc Med **98,** 341, 2005.
27. Gimble, J.M., Katz, A.J., and Bunnell, B.A. Adipose-derived stem cells for regenerative medicine. Circ Res **100,** 1249, 2007.
28. Bilheimer, D.W., Goldstein, J.L., Grundy, S.M., Starzl, T.E., and Brown, M.S. Liver transplantation to provide low-density-lipoprotein receptors and lower plasma cholesterol in a child with homozygous familial hypercholesterolemia. N Engl J Med **311,** 1658, 1984.

Address correspondence to:
Akifumi Matsuyama, M.D., Ph.D.
Department of Somatic Stem Cell Therapy and Health Policy
Foundation for Biomedical Research and Innovation
TRI305, 1-5-4 Minatojima-minamimachi, Chuo-ku
Kobe 650-0047
Japan

E-mail: akifumi-matsuyama@umin.ac.jp

Received: March 7, 2010
Accepted: August 9, 2010
Online Publication Date: September 21, 2010

Impaired Myocardium Regeneration With Skeletal Cell Sheets—A Preclinical Trial for Tissue-Engineered Regeneration Therapy

Shigeru Miyagawa,[1] Atsuhiro Saito,[2] Taichi Sakaguchi,[1] Yasushi Yoshikawa,[1] Takashi Yamauchi,[1] Yukiko Imanishi,[1] Naomasa Kawaguchi,[3] Noboru Teramoto,[4] Nariaki Matsuura,[3] Hidehiro Iida,[4] Tatsuya Shimizu,[5] Teruo Okano,[5] and Yoshiki Sawa[1,6]

Background. We hypothesized that autologous skeletal cell (SC) sheets regenerate the infract myocardium in porcine heart as a preclinical trial.

Methods and Results. The impaired heart was created by implantation of ameroid constrictor on left anterior descending for 4 weeks. SCs isolated from leg muscle were cultured and detached from the temperature-responsive domain-coated dishes as single monolayer cell sheet at 20°C. The following therapies were conducted: SC sheets (SC group, n=5); sham (C group n=5). Echocardiography demonstrated that cardiac performance was significantly improved in the SC group 3 and 6 months after operation (fractional area shortening, 3 months; SC vs. C=49.5±2.8 vs. 24.6±2.0%, $P<0.05$) and left ventricle dilatation was well attenuated in the SC group. Color kinesis index showed that distressed regional diastolic and systolic function in infarcted anterior wall was significantly recovered (SC vs. C=57.4±8.6 vs. 30.2±4.7%, $P<0.05$, diastolic: 58.5±4.5 vs. 35.4±6.6%, $P<0.05$, systolic). Factor VIII immunostains demonstrated that vascular density was significantly higher in the SC group than the C group. And % fibrosis and cell diameter were significantly lower in the SC group. And hematoxylin-eosin staining depicted that skeletal origin cells and well-developed-layered smooth muscle cells were detected in the implanted area. Positron emission tomography showed better myocardial perfusion and more viable myocardial tissue in the distressed myocardium receiving SC sheets compared with the myocardium receiving no sheets.

Conclusions. SC sheet implantation improved cardiac function by attenuating the cardiac remodeling in the porcine ischemic myocardium, suggesting a promising strategy for myocardial regeneration therapy in the impaired myocardium.

Keywords: Cells, Heart failure, Myocardial infarction, Tissue, Transplantation.

(*Transplantation* 2010;90: 364–372)

Despite the recent remarkable progress in medical and surgical treatments for heart failure, end-stage heart failure has been still a major cause of death worldwide. After myocardial infarction, the myocardium is capable of a limited regenerative capacity and no medication or procedure used clinically has shown efficacy in regenerating myocardial scar tissue with functioning tissue. Thus, there is a need for new therapeutics to regenerate damaged myocardium.

Recent developments in tissue engineering show promise for the creation of functional cardiac tissues without the need for biodegradable alternatives for the extracellular matrix (*1*). And we reported that cardiomyocyte sheets have been developed by using temperature-responsive culture dishes and these sheets survived in the back of nude rats and showed a spontaneous contraction over a long period of time (*2*). Recent reports suggested that cardiomyocyte sheets integrated with the impaired myocardium and improved cardiac performance in a rat model of ischemic myocardium (*3*).

This work was supported by a Grant-in-Aid for Scientific Research in Japan.

[1] Division of Cardiovascular Surgery, Department of Surgery, Faculty of Medicine, Osaka University Graduate School of Medicine, Suita, Osaka, Japan.

[2] Medical Center for Translational Research, Osaka University Hospital, Osaka, Japan.

[3] Department of Pathology, School of Allied Health Science, Faculty of Medicine, Osaka University Graduate School of Medicine, Suita, Osaka, Japan.

[4] Department of Investigative Radiology, National Cardiovascular Center Research Institute, Tokyo, Japan.

[5] Tokyo Women's Medical University Institute of Advanced Biomedical Engineering and Science, Tokyo, Japan.

[6] Address correspondence to: Yoshiki Sawa, M.D., Department of Cardiovascular Surgery, Osaka University Graduate School of Medicine, 2-2 Yamada-oka, Suita, Osaka 565-0871, Japan.

E-mail: sawa@surg1.med.osaka-u.ac.jp

S.M. participated in the writing of the paper; A.S. participated in research design; T.S. and Y.Y. participated in data analysis; T.Y., Y.I., N.K., and N.T. participated in the performance of research; N.M., H.I., T.S., T.O., and Y.S. participated in research design.

Received 15 December 2009. Revision requested 2 January 2010.

Accepted 6 May 2010.

ISSN 0041-1337/10/9004-364

DOI: 10.1097/TP.0b013e3181e6f201

And more recently, in the aim of clinical application, nonligature implantation of skeletal myoblast sheet regenerated the damaged myocardium and improved global cardiac function by attenuating the cardiac remodeling in the rat ligation model (*4*) and dilated cardiomyopathy hamster model (*5*). This cell delivery system by using cell sheets implantation showed better restoration of damaged myocardium compared with needle injection (*4*, *5*). Moreover, grafting of skeletal myoblast sheets attenuated cardiac remodeling and improved cardiac performance in pacing-induced canine heart failure model (*6*).

Given this body of evidence, we hypothesized that the autologous skeletal cell (SC) sheet implantation might remodel the chronic heart failure caused by ischemic injury.

Therefore, this preclinical study using Swine model was designed to test therapeutic effectiveness.

MATERIALS AND METHODS

Myocardial Infarction Model

"Principles of Laboratory Animal Care" formulated by the National Society for Medical Research and the "Guide for the Care and Use of Laboratory Animals" prepared by the Institute of Laboratory Animal Resource and published by the National Institutes of Health (NIH Publication No. 86-23, revised 1985). This animal experiment was approved by the Animal Care Committee of Osaka university graduate school of medicine. We induced acute myocardial infarction of 10 swine (20 kg, KEARI, Japan) by the following method. Swine were preanesthetized by intramuscular injection of ketamine hydrochloride 20 mg/kg (Ketalar, Sankyo, Japan) and xylazine 2 mg/kg (Seractar, Bayer). Animals were positioned spine and a 22-gauge indwelling needle (Surflo F&F, Terumo, Tokyo, Japan) was inserted in the central vein of the auricle. A three-way cock (Terufusion TS-TR2K, Terumo, Tokyo, Japan) was attached to the external cylinder of the indwelling needle, and an extension tube was connected for continuous anesthetic injection. The animals were intubated with an endotracheal cannula (6 Fr, Sheridan) using a pharyngoscope and then connected to an artificial respirator (Harvard, USA) by the cannula. Artificial respiration was implemented at a stroke volume of 200 to 300 mL/stroke and a stroke frequency of 20/min. The animals were continuously drip injected with propofol 6 mg/kg/hr (Diprivan, AstraZeneca) and vecuronium bromide 0.05 mg/kg/hr (Musculux, Sankyo Yell Yakuhin Co., Ltd., Japan) using a syringe pump (Terufusion TE-3310N, Terumo, Japan). The animal was then fixed in a recumbent position, so that the left thorax was exposed, and the outer layer of skin and muscles between the third and fourth ribs were dissected. After confirming the cutting into the thoracic cavity, the distance between the third and fourth ribs was widened with a rib spreader to allow a direct view of the left auricle and the LAD coronary artery. The pericardium was dissected along the LAD from the upper part of the left auricle (~6 cm) to expose the myocardium around the LAD. LAD on the proximal side below the left auricle from the myocardium was exfoliated for approximately 1 cm, and then a small amount of lidocaine hydrochloride jelly (Xylocaine jelly, AstraZeneca) was applied to allow for anesthetizing the area. An ameroid constrictor (COR-2.50-SS, Research Instruments) was then fit using No. 1 or 2 suture. The chest cavity was closed to end the procedures. The animals were randomly divided into two treatment groups: the first received autologous SC sheet implantation (SC group, n=5). For control, we have performed sham operation (C group, n=5).

Preparation of Skeletal Cell Sheets for Grafting

One week after implantation of ameroid constrictor on LAD, skeletal muscle weighing approximately 5 g was removed from the pretibial region with the porcine under general anesthesia. Following the addition of trypsin-ethylenediaminetetraacetic acid (Gibco, Grand Island, NY), excessive connective tissue was carefully removed to minimize the content of contaminating fibroblasts, and the muscle tissue was minced until the fine pieces formed a homogeneous mass. The specimens were then incubated at 37°C in shaker bath with 0.5% type 1 collagenase (Gibco) in Dulbecco's modified Eagle's medium (Gibco). After brief placement, the fluid was collected, and the same volume of culture medium, SkBM (Cambrex, Walkersville, MD) supplemented with fetal bovine serum (Thermo Trace, Melbourne, Australia), was added to halt the enzymatic digestion process. The cells were collected by centrifugation, and the putative SCs were seeded into 150 cm^2 polystyrene flasks after removal of fibroblasts by sedimentation for a few hours and cultured in SkBM at 37°C. During the culture process, we maintained cell densities at less than 70% confluence by carrying out passaging of cells for one time to prevent SCs from premature differentiation and fusion process resulting in myotubes formation. When the cells become approximately 70% confluent after 10 to 11 days cultivation, the cells were dissociated from the flasks with trypsin-ethylenediaminetetraacetic acid and reincubated on 100 mm temperature-responsive culture dishes (Cellseed, Tokyo, Japan) at 37°C with the cell numbers adjusted to 1×10^7 per dish. More than 90% of these cells were desmin positive (Fig. 1). After 4 days, the dishes were removed to refrigerator set at 20°C, and left there for approximately 30 min. During that time, the SC sheets detached spontaneously from the surfaces. Each sheet had a diameter of 30 to 40 mm and consisted of layers of SCs; the sheets were approximately 100-μm thick in cross-sectional views (Fig. 1). Approximately 10 sheets were obtained from the 5 g of skeletal muscle.

Implantation of Skeletal Cell Sheets

Autologous SC sheet implantation was performed in the swine 4 weeks after LAD ligation. Swine were anesthetized as mentioned above. The swine were exposed through the sternum. The infarct area was identified visually on the basis of surface scarring and abnormal wall motion. In the SC group, we implanted 10 SC sheets into the infarcted myocardium. The control group was treated similarly but received no SC sheets. Because pilling up four or more sheets caused the central necrosis of the myoblasts presumably because the lack of in oxygen supply, we decided to pile two or three layers of the SC sheet over the broad surface of the impaired heart.

Measurement of Cardiac Function

Swine were anesthetized as mentioned above. Cardiac ultrasonography was performed with a commercially available echocardiograph, SONOS 5500 (PHILIPS Electronics, Tokyo, Japan). A 3-MHz annular array transducer was placed on a layer of acoustic coupling gel that was applied to the left hemithorax. Swine were examined in a shallow left lateral decubitus position. The heart was first imaged in the two-dimensional mode in short-axis views at the level of the largest left ventricle (LV) diameter. The calculation of the LV volume was based on the LV short-axis area using AQ system (*7*). And fractional area shortening (FAS) of the LV diastolic was calculated as follows:

$$\text{FAS}\ (\%) = [(\text{LVend-diastolic area} - \text{LV end-systolic area [ESA]})/\text{LV end-diastolic area}] \times 100$$

These data are presented as the average of measurements of two or three selected beats.

Quantification of Regional Diastolic and Systolic Function by Color Kinesis

Diastolic CK images were obtained using a commercially available ultrasound system (SONOS 5500, Philips Medical Systems) from the LV midpapillary short-axis view for the determination of wall motion asynchrony as previously reported (*8*). CK examined every image pixel within the region of interest, which was drawn around the LV cavity, classifying it as blood or tissue based on integrated backscatter data. During diastole, each pixel was tracked into the next frame, and pixel transitions from endocardium to blood were detected and interpreted as diastolic endocardial motions. These pixel transitions were encoded using a color hue specific to each consecutive video frame, so that each color represents the excursion of that segment during a 33-ms period of time. The sites of regional LV diastolic wall motion or regions of interest were set on the basis of standard segmentation models: anterior, lateral, posterior, inferior, anteroseptal wall. The CK diastolic index was defined as the LV segmental filling fraction

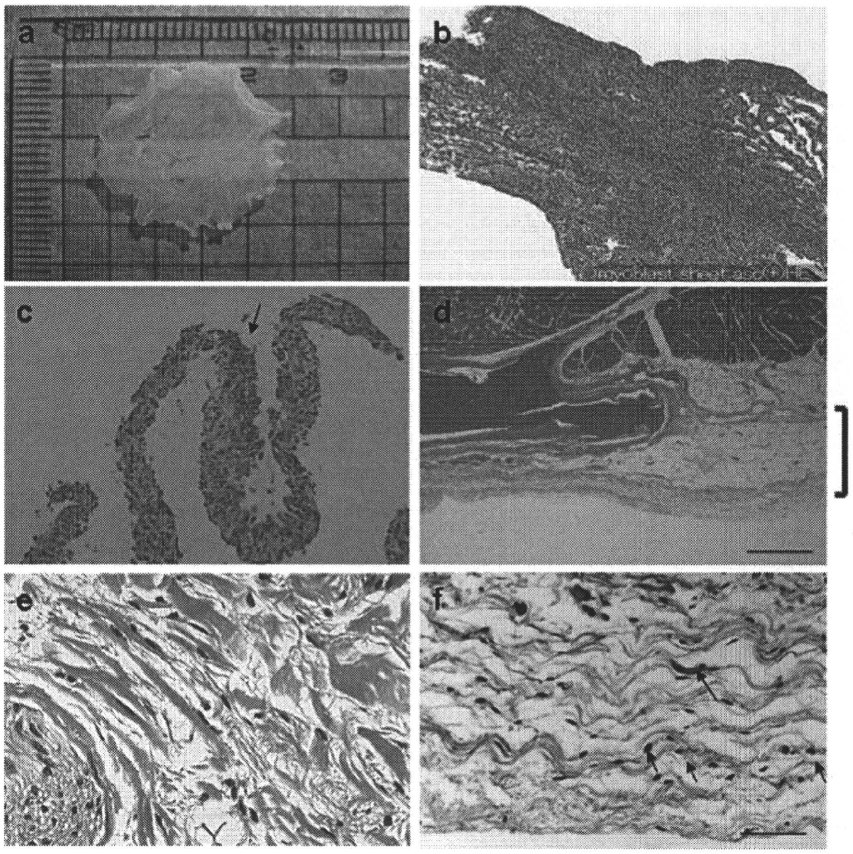

FIGURE 1. Histological characteristics of skeletal cell (SC) sheet. (a) SC sheet detached from the Poly (*N*-isopropylacrylamide)-grafted polystyrene by lowering the temperature. Its size is approximately 3 cm×2 cm^2. (b) Hematoxylin-eosin (H&E) stain; cross-sectional views of SC sheet in vitro. SC sheet demonstrates homogeneous heart-like tissue. (c) Not so many smooth muscle cells were detected in the SC sheets. The *arrow* indicates the smooth muscle cells in the SC sheet. (d) H&E stain revealed that SC sheets attached on the surface of epicardium. *Left square bracket* indicates implanted SC sheets. (e) Oval-shaped cells that showed positive for eosin in cytoplasm were detected in the SC group microscopically in some layers over epicardium. (f) Elastica Masson Goldner showed that oval-shaped cells that supposed to origin from skeletal tissue exist in the transplantation site. *Arrows* indicate oval-shaped cells that suppose to be originated form skeletal tissue.

during the first 30% of the diastolic filling time (LV segmental cavity area expansion during the first 30% of diastole, divided by the segmental end-diastolic LV cavity area expansion, expressed as a percentage). We introduced the use of color kinesis method that displays endocardial motion in real time to evaluate the regional systolic function (*8*).

Histopathology

LV myocardium specimens were obtained 6 months after the SC sheet implantation. Each specimen was fixed with 10% buffered formalin and embedded in paraffin. A few serial sections were prepared from each specimen and stained with hematoxylin-eosin (H&E) stain and elastica Masson-Goldner for histological examination or with Masson's trichrome stain to assess the collagen content.

To label vascular endothelial cells so that the blood vessels could be counted, immunohistochemical staining of factor VIII-related antigen was performed according to a modified protocol. Frozen sections were fixed with a 2% paraformaldehyde solution in phosphate-buffered saline (PBS) for 5 min at room temperature, immersed in methanol with 3% hydrogen peroxide for 15 min, then washed with PBS. The samples were covered with bovine serum albumin solution (DAKO LSAB Kit DAKO CORPORATION, Denmark) for 10 min to block nonspecific reactions. The specimens were incubated overnight with an Enhanced Polymer One-Step Staining (EPOS)-conjugated antibody against factor VIII-related antigen coupled with horseradish peroxidase (DAKO EPOS Anti-Human Von Wille brand Factor/HRP, DAKO, Denmark). After the samples were washed with PBS, they were immersed in diaminobenzidine solution (0.3 mg/mL diaminobenzidine in PBS) to obtain positive staining. Ten different fields at 200× magnification were randomly selected, and the number of the stained vascular endothelial cells in each field was counted under a light microscope. The result was expressed as the number of blood vessels per square millimeter.

The following antibodies against smooth muscle cells and skeletal myosin (slow) were used to evaluate the existence of SCs: primary antibodies, anti-smooth muscle actin (clone 1A4, DAKO) antiskeletal myosin (slow) (clone NOQ7.5.4D, Sigma); secondary antibodies, anti-mouse Ig biotinylate (DAKO).

Picro-sirius red staining for the assessment of myocardial fibrosis or periodic acid-Schiff staining for that of cardiomyocyte hypertrophy was performed as described (*9*).

Positron Emission Tomography Procedure

We performed positron emission tomography (PET) studies on pigs which were transplanted SC sheets and control by using ^{15}0-water and ^{18}F-FDG. The pigs were anesthetized by the introduction of pentobarbital followed by continuous inhalation of propofol (4 mg/kg/hr) and were placed supine on the bed of the scanner. PET was performed using a HEADTOME-III tomograph (Shimadzu, Kyoto, Japan) and data were analyzed as described elsewhere (*10*).

Holter Electrocardiography

To evaluate arrhythmia we used Holter electrocardiography (ECG) for 24 hours. We checked arrhythmia by checking the number of ventricular premature beat after SC sheet implantation in myocardial infarction porcine (n=3).

Data Analysis

Data are expressed as means ± SEM and subjected to multiple analysis of variance (ANOVA) using the StatView 5.0 program (Abacus Concepts, Berkeley, CA). Echocardiographic data were first analyzed by two-way repeated measurement ANOVA for differences across the whole time course, and one-way ANOVA with the Tukey-Kramer posthoc test was used to verify the significant for the specific comparison at each time point. To assess the significance of the differences between individual groups concerning other numeral data, statistical evaluation was performed with an unpaired *t* test. Statistical significance was determined as having a *P* value less than 0.05.

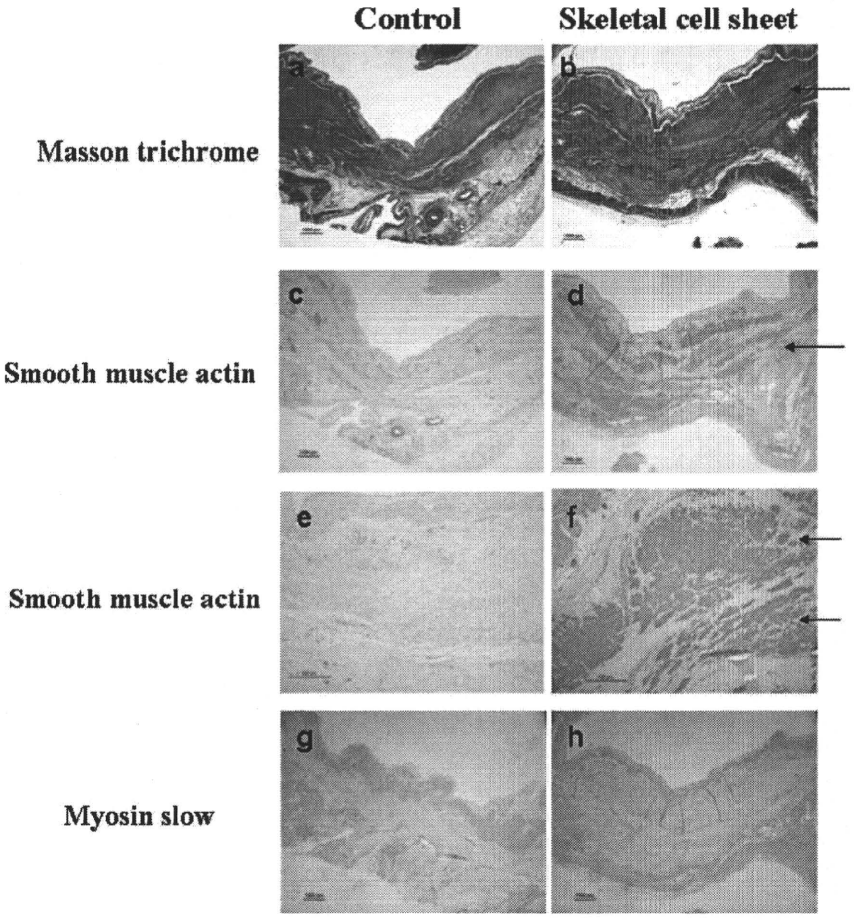

FIGURE 2. The detection of a large quantity of skeletal cells (SCs) in the center of the scar. (a and b) Masson trichrome staining reveals that some layered muscles are detected in the center of the scar in the SC sheet transplantation group, whereas not in the control. (c–f) Smooth muscle actin staining demonstrated that well-developed smooth muscle cells occupied in the center of the scar in the SC sheet transplantation group, whereas only smooth muscle cells which are formed vasculature are detected in the control. (g and h) Slow-type myosin staining showed that no positive cells exist in the center of the scar. This means that SCs which are detected in the center of the scar are not the residual myocyte after infarction.

RESULTS

Characteristics of Myoblast Sheet

We obtained monolayered myoblast sheets by lowering the temperature, which released them from the Poly(*N*-isopropylacrylamide)-grafted polystyrene. Its size is approximately 3 cm×2 cm^2 (Fig. 1a). H&E staining demonstrated that SC sheet contained a lot of SCs and SC sheets had an appearance of homogenous tissue, which thickness of one SC sheet was approximately 100 μm (Fig. 1b). Some smooth muscle cells are detected in the SC sheets, but those cells are not majority (Fig. 1c).

Histological Assessment

H&E staining demonstrated that transplanted SC sheets were attached in the epicardium (Fig. 1d) and oval-shaped cell that showed positive for eosin in cytoplasm were detected in the SC group microscopically in some layers over epicardium (Fig. 1e). Elastica Masson-Goldner showed that oval-shaped cells that supposed to origin from skeletal tissue exist in the transplantation site (Fig. 1f). These cells were not seen in the control group. And the SC group demonstrated decrease in the cross-sectional LV area compared with the C groups (Fig. 2a). Masson's trichrome staining showed that clustered SCs were detected in the center of the scar, whereas clustered SCs were not detected in the C group (Fig. 2a, b). Many clusters of well-developed smooth muscle cells exist in the center of the whole scar in the SC group, whereas in the C group, smooth muscle cells which formed vasculature exist in the scar (Fig. 2c–f). Although slow-type myosin-positive cells exist only on the endocardium and epicardium, those cells were not detected in the center of scar (Fig. 2g,h). So these figures depict that the skeletal muscle cells that exist in the center of the scar is not residual myocyte after infarction.

Quantification of Histopathology

In the SC group, vascular density was found to be significantly higher than in the C groups (SC vs. C=217.1±30.2 vs. 114.2±18.2 /field; $P<0.05$) (Fig. 3b).

Picro-sirius red staining demonstrated that % fibrosis was significantly reduced in the SC group compared with the C group (SC vs. C=1.6±0.2 vs. 3.1±0.3%; $P<0.05$) (Fig. 3b). Periodic acid-Schiff staining showed that cell diameter was significantly shorter in the SC group than the C group (SC vs. C=10.7±0.3 vs. 18.3±1.4 μm; $P<0.05$) (Fig. 3b).

These histological findings were universally identified in the native myocardial tissue without distinction of distance from the grafted region.

Functional Assessment of the Infarcted Myocardium

The FAS and LV end-ESA scores at baseline were not significantly different between the two groups.

Three months after the implantation, two-dimensional echocardiography showed significant improvement of the

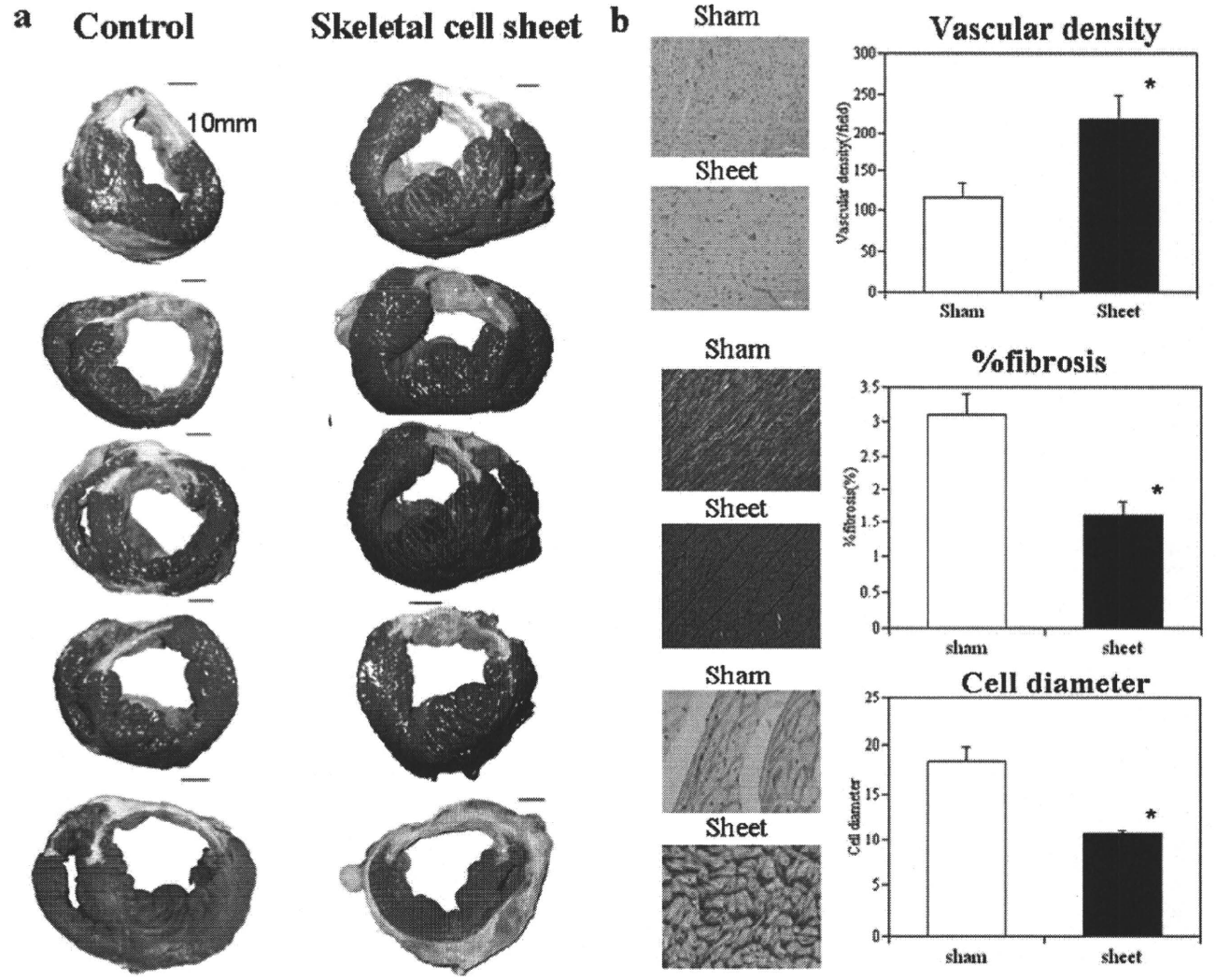

FIGURE 3. Macroscopic images of impaired myocardium receiving skeletal cell (SC) sheets and histological evaluation. (a) In the SC group, the anterior wall has recovered compared with the C group. In the SC group, the short axis area of the left ventricle (LV) is small compared with the C groups. In contrast, the C group shows a dilated LV and the anterior wall is thinner than in the SC groups. (b) Histological evaluation. Vascular density: the SC group showed a significant improvement in vascular density as assessed by immunostaining for the factor VIII-related antigen. *P less than 0.05 vs. C. The ratio of fibrosis-occupied area (% fibrosis) at a site remote from the infarcted heart region: picro-sirius red staining demonstrated that % fibrosis at a site remote from the infarcted heart region was significantly reduced in the SC group compared with the C group. *P less than 0.05 vs. C. The diameter of cardiomyocyte: the diameter of cardiomyocyte is significantly shorter in the SC group than the C group. *P less than 0.05 vs. C.

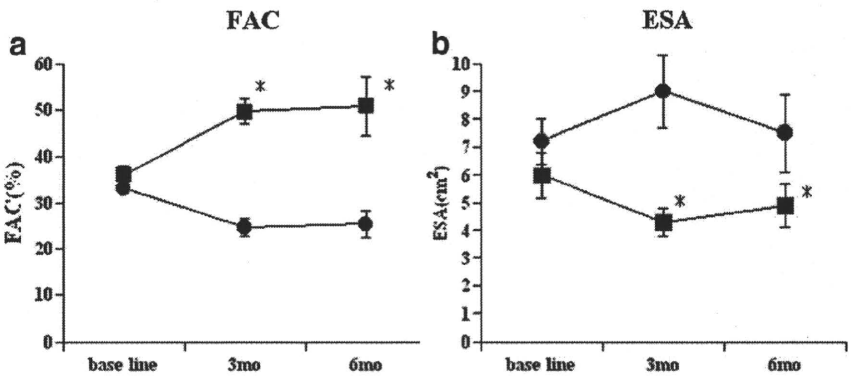

FIGURE 4. Global functional effects of infarcted myocardium receiving the implant. Global systolic function assessed by the fractional area shortening (FAS) (a) was significantly improved in the skeletal cell (SC) group 3 months after transplantation, and these functional improvements were preserved 6 months after SC sheet implantation. (b) The end-systolic area (ESA) was significantly smaller in the SC group than in the C groups 3 and 6 months after implantation. *P less than 0.05 vs. C, ■: SC sheet, ●: control.

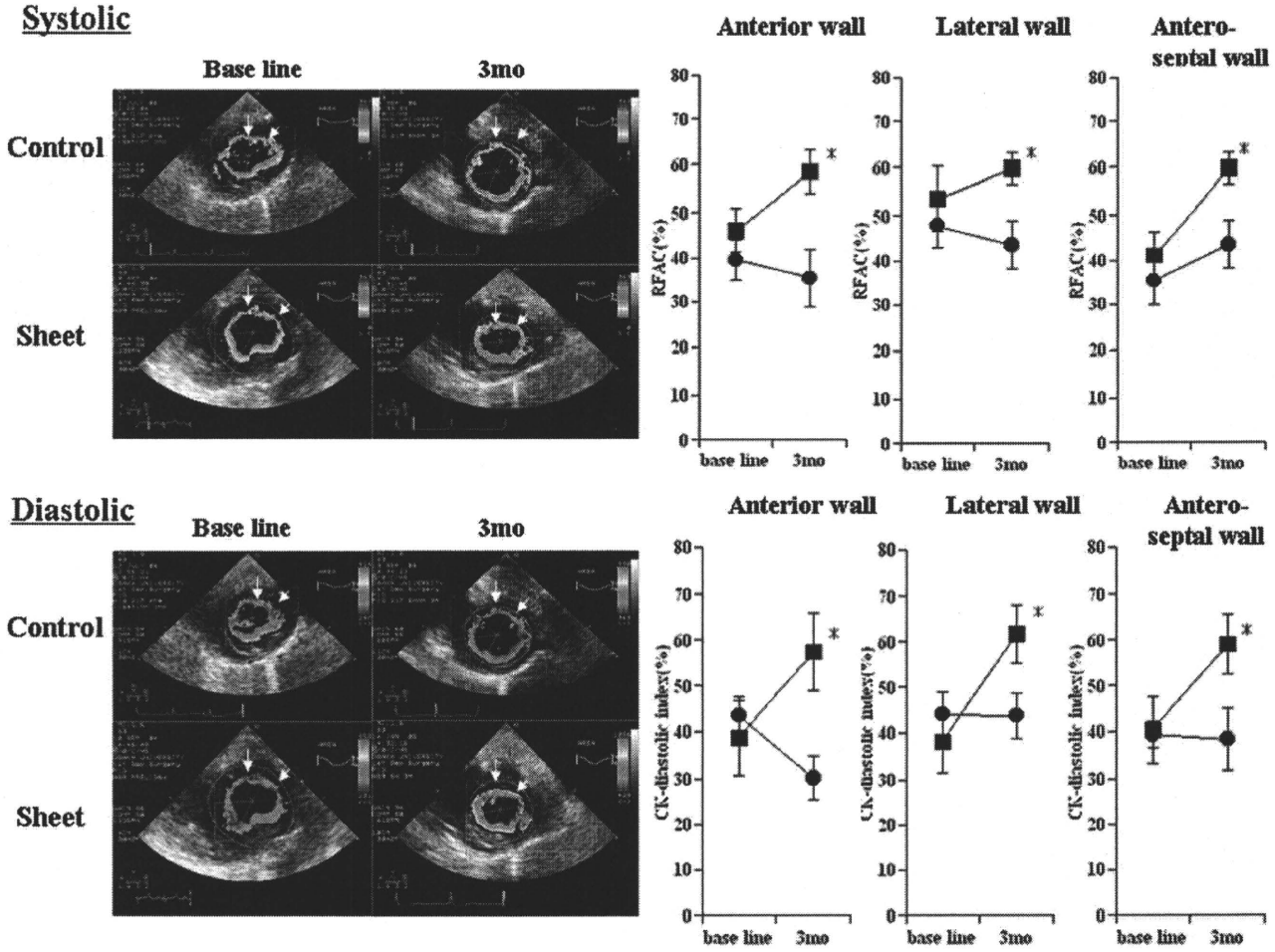

FIGURE 5. Systolic function: regional systolic function was significantly recovered in the skeletal cell (SC) group 3 months after implantation compared with the C group in the anterior, lateral, and anteroseptal wall. *P less than 0.05. Diastolic function: regional dysfunction was significantly recovered in the SC group 3 months after implantation compared with the C group in the anterior, lateral, and anteroseptal wall. Before treatment, diastolic dysfunction was observed in the infarction area of myocardium and the regional delayed relaxation was detected in the remote site of infarction by color kinesis. But this phenomenon was disappeared after SC sheet implantation. *P less than 0.05, ■: SC sheet, ●: control.

FAS (Fig. 4a) in the SC group compared with the C group (SC vs. C=49.5±2.8 vs. 24.6±2.0%, $P<0.05$). These functional improvements were preserved 6 months after implantation (SC vs. C=50.8±6.4 vs. 25.3±2.8%, $P<0.05$). The ESA was significantly smaller in the SC group than in the C group 3 months after the implantation (SC vs. C=4.3±0.5 vs. 9±1.3 cm^2, $P<0.05$) (Fig. 4b). These attenuation of LV dilatation were preserved 6 months after implantation (SC vs. C=4.9±0.8 vs. 7.5±1.4 cm^2, $P<0.05$). During this long-term observation, all SC sheet-treated animals were alive and exhibited no malignant arrhythmia assessed by 24-hour Holter ECG once a week (data not shown).

Before treatment, diastolic dysfunction was observed in the infarction area of myocardium and the regional delayed relaxation was detected in the remote site of infarction by color kinesis. After 3 months after implantation, CK-diastolic index in the lateral (SC vs. C=61.7±6.4 vs. 43.7±4.8%, $P<0.05$), anterior (SC vs. C=57.4±8.6 vs. 30.2±4.7%, $P<0.05$), and anteroseptal (SC vs. C=59±6.6 vs. 38.4±6.6%, $P<0.05$) segment were significantly ameliorated in the SC group compared with the C group, and regional systolic function in transplanted site was significantly improved in the SC group while not in the C groups (SC vs. C: lateral, 59.8±3.3 vs. 43.6±5.4%, $P<0.05$; anterior, 58.5±4.5 vs. 35.4±6.6%, $P<0.05$; anteroseptal, 59.8±3.3 vs. 43.6±5.4%, $P<0.05$), respectively (Fig. 5).

We could detect no ventricular premature beat for 24 hr by the Holter ECG in three myocardial infarction porcine received SC sheets.

Regional Myocardial Blood Flow and Residual Myocardial Tissue

PET study by using ^{15}0-water showed that the myocardial water-perfusable tissue fraction and myocardial blood flow were higher in the anterior wall where SC sheets were implanted compared with the myocardium receiving no sheets. These data depict that myocardial blood flow was better and microcirculation in the infarcted myocardium was preserved in the SC sheets implanted myocardium. PET study by using ^{18}F-FDG revealed that more viable myocardial tis-

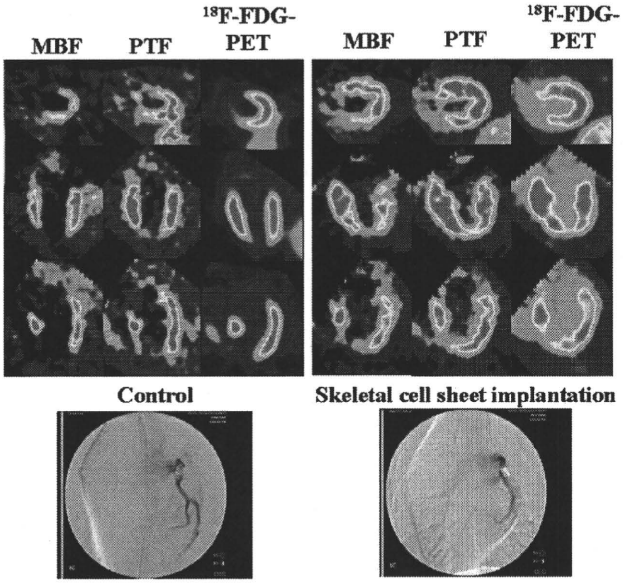

FIGURE 6. Positron emission tomography (PET) study revealed that perfusable tissue fraction (PTF) and myocardial blood flow (MBF) were higher and more viable myocardial tissues were preserved in the skeletal cell sheets implanted site compared with the myocardium receiving no sheets.

sues were preserved in the skeletal sheet implanted myocardium compared with the myocardium receiving no sheets. Coronary angiography revealed that LAD was occluded by the ameroid constrictor in both cases (Fig. 6).

DISCUSSION

Over the past several years, increasing awareness of the shortcomings of heart transplantation and left ventricular assist system implantation has led cardiovascular surgeons to consider alternative means of treating end-stage heart failure. In clinical setting, cellular cardiomyoplasty has been reported to have the potential of fundamental regenerative capability and has already been introduced in clinical trials with skeletal myoblast (*11*) or bone marrow mononuclear cells (*12*), and results suggest that it is a relatively feasible and safety therapy as a therapeutic angiogenesis. In this setting, cardiac tissue implantation was proposed to the treatment of end-staged heart failure as a new concept of regenerative therapy and experimentally some groups depicted it's effectiveness in the damaged myocardium (*13*, *14*). We also reported that cell sheets have great impacts on restoration of damaged myocardium in the rat infarction model (*3*, *4*) and dilated cardiomyopathy hamster (*5*). To convince the effectiveness of cell sheets in preclinical trial, we examined whether autologous SC sheets implantation might become one of the armamentarium of regenerative therapy for chronic heart failure caused by myocardial infarction in the porcine model.

The potential added advantages of the cell sheet implantation method include the implantation of a high number of cells with minimum cell loss. In contrast, the injection method is associated with a high loss of cells or surface proteins due to the trypsin treatment. Despite a high number of cell loss in needle injection, the cell sheet implantation method might provide the advantages of a higher number of cell implantation without cellular community destruction, leading the more improvement of cardiac performance rather than cell injection method (*4*). In case of needle injection, inflammation accompanied with destruction of myocardium induced by needle injection promotes graft death after cell transplantation (*15*).

To examine the effects of the SC sheet implantation therapy, we analyzed cardiac function and performed a histological assessment of the infarcted heart after SC sheet transplantation in a swine infarction model. SC sheet implantation therapy significantly induced angiogenesis, reduction of fibrosis histologically. And cell diameter of host myocyte was significantly attenuated its hypertrophy compared with the no treatment group. PET study revealed the better regional blood perfusion and better regional myocardial viability in the myocardium receiving cell sheets compared with the myocardium receiving no sheets.

Moreover, SC sheet implantation induced functional recovery of damaged myocardium. Especially, we demonstrated that the regional diastolic and systolic dysfunction was well recovered in the sheet implanted group. Before treatment, diastolic dysfunction of infarcted area and regional delayed relaxation of noninfarcted site were detected by color kinesis in the porcine infracted myocardium. After treatment, diastolic dysfunction of infarcted site was significantly recovered and the phenomenon of regional delayed relaxation in noninfarcted site was not seen. Presumably, implanted elastic myoblast sheets and a large quantity of well-developed smooth muscle cells, which are detected in the center of the scar, improved the regional diastolic dysfunction of implanted site. Although SC sheet can not contract in vivo after implantation, this recovery of diastolic disassociation of LV might result in the recovery of systolic dysfunction.

To the best of our knowledge, this is the first report in which tissue-engineered SC sheets implantation was successfully used to improve cardiac performance in a large animal model of ischemic myocardium according to the Laplace's theory.

The mechanisms of the restoration of damaged myocardium by SC sheet implantation might be complicated and many pathways might affect the recovery of ischemic myocardium. Recent reports depict that cell sheets enhance the recruitment of hematopoietic stem cells through the release of stromal-derived factor 1 (*4*). The fact of thicker anterior wall and the improvement of regional function might depend on both the recruitment of cytokine releasing stem cells, survival of grafted cells, and well-developed smooth muscle cells. And these cells might have good elasticity and these elastic cells and tissues softened the stiffness of anterior wall in association with the attenuating fibrosis even in the infarct area. This reduced stiffness of anterior wall might lead to the improvement of the diastolic dysfunction. Transplanted SCs cannot differentiate into cardiomyocyte anymore, but regional systolic function improved in the transplanted site. Probably, the improvement of regional diastolic function due to elastic cells might be responsible for the restoration of regional systolic dysfunction. Recent reports demonstrated that regional left ventricular myocardial relaxation was closely related to regional myocardial contraction (*16*) and the improvement of regional myocardial relaxation leads to the

recovery of global diastolic function (*17*). Moreover, the improvement of regional systolic function is closely related to global systolic function (*18*). We assume that this theory about the relationship between diastolic and systolic function is one of the mechanisms about the improvement of diastolic and systolic function in the cell sheet transplanted myocardium.

Question is why the well-developed smooth muscle cells exist in the center of the scar in the SC sheet group after transplantation despite a small quantity of smooth muscle cells in the SC sheet? Does a small quantity of smooth muscle cells in the SC sheet proliferate after transplantation? Do progenitor cells in the SC sheet differentiate to smooth muscle cells? Do progenitor cells or smooth muscle cells in the host myocardium migrate to the implanted site and proliferate? To the regret, there is no data to answer these questions exactly in this article and more detailed studies are needed to elucidate this important question.

Some reports depicted that the expression of hepatocyte growth factor (HGF) in the myoblast sheet transplanted ischemic myocardium is higher compared with the nontransplanted ischemic myocardium (*4*). HGF has an antifibrotic activity both through the activation of a matrix degradation pathway (*19*), restoration of cytoskeletal proteins on cardiomyocyte (*20*), and induce angiogenesis in the ischemic myocardium (*21*). Our study demonstrated that % fibrosis was significantly reduced in the SC sheet transplanted group. This paracrine secretion of HGF from SC sheets might attribute the reduction of % fibrosis. In our study, much more factor VIII-positive cells are detected in the SC sheet transplanted myocardium. This might be induced by paracrine secretion of HGF and angiogenesis might rescue the ischemic host cardiomyocyte and bring about the improvement of the distressed function of host cardiomyocyte. The distressed cytoskeletal proteins on the cardiomyocyte in the ischemic myocardium might be reorganized by the HGF secreted from skeletal sheet and the restoration of cytoskeletal proteins might lead to the improvement of cardiac function. And some reports demonstrated that myoblast sheets maintain the distressed cytoskeletal proteins on the host cardiomyocyte in the dilated cardiomyopathy hamster model (*5*). Consequently, cell sheet treatment is appropriate for recovery of ischemic cardiomyopathy. Recent research works demonstrated that several regenerative factors such as insulin-like growth factor-1 (*22*) and Thymosin b4 (*23*) were expressed in the rat ischemic myocardium model after myoblast sheet implantation by reverse-transcriptase polymerase chain reaction analysis (data not shown). After myoblast sheet transplantation to ischemic myocardium, several regenerative factors are expressed in the transplanted site, and these long-term and low-dosed expressed regenerative factors might cooperatively restore the damaged myocardium.

We could find no ventricular premature beat analyzed by Holter ECG after SC sheet implantation. We have already proved that in the rat infarction model, arrhythmia is less in the SC sheet implantation group compared with the needle injection group and this work represented that more monocyte chemotactic protein-1-positive cells and CD11b (macrophage marker)-positive cells were detected in the needle injection group compared with SC sheet implantation (data not shown). We speculate that needles destroy the myocardium and this destroyed myocardium may induce the inflammation and this inflammation may induce the arrhythmia. Conversely, SC sheet implantation technique normally doses not destroy the myocardium when they are implanted to recipient heart. Moreover, SC sheet will survive on the epicardium and electrical wave originated from implanted myoblasts may not deliver to the recipient myocardium directly. But when we implant myoblasts by needle injection, implanted myoblasts survive in the center of the myocardium and electrical wave will deliver to the myocardium directly, leading to the arrhythmia.

In conclusion, we have preclinically demonstrated SC sheets produced histologically and functionally apparent prevented the deterioration of the impaired myocardium in the swine model. These data provide a basis for attempting clinical cell sheet implantation in ischemic disease as the armamentarium to promote the regeneration of chronic heart failure caused by myocardial infarction.

ACKNOWLEDGMENTS

The authors thank Shigeru Matsumi and Masako Yokoyama for their excellent technical assistance.

REFERENCES

1. Shimizu T, Yamato M, Akutsu T, et al. Fabrication of pulsatile cardiac tissue grafts using a novel 3-dimensional cell sheet manipulation technique and temperature-responsive cell culture surfaces. *Circ Res* 2002; 90: e40.
2. Shimizu T, Sekine H, Isoi Y, et al. Long-term survival and growth of pulsatile myocardial tissue grafts engineered by the layering of cardiomyocyte sheets. *Tissue Eng* 2006; 12: 499.
3. Miyagawa S, Sawa Y, Sakakida S, et al. Tissue cardiomyoplasty using bioengineered contractile cardiomyocyte sheets to repair damaged myocardium: Their integration with recipient myocardium. *Transplantation* 2005; 80: 1586.
4. Memon IA, Sawa Y, Fukushima N, et al. Repair of impaired myocardium by means of implantation of engineered autologous myoblast sheets. *J Thorac Cardiovasc Surg* 2005; 130: 1333.
5. Kondoh H, Sawa Y, Miyagawa S, et al. Longer preservation of cardiac performance by sheet-shaped myoblast implantation in dilated cardiomyopathic hamsters. *Cardiovasc Res* 2006; 69: 466.
6. Hata H, Matsumiya G, Miyagawa S, et al. Grafted skeletal myoblast sheets attenuate myocardial remodeling in pacing-induced canine heart failure model. *J Thorac Cardiovasc Surg* 2006; 132: 918.
7. Mor-Avi V, Vignon P, Bales AC, et al. Acoustic quantification indexes of left ventricular size and function: Effects of signal averaging. *J Am Soc Echocardiogr* 1998; 11: 792.
8. Ishii K, Miwa K, Makita T, et al. Prolonged postischemic regional left ventricular delayed relaxation or diastolic asynchrony detected by color kinesis following coronary vasospasm. *Am J Cardiol* 2003; 91: 1366.
9. Fukui S, Kitagawa-Sakakida S, Kawamata S, et al. Therapeutic effect of midkine on cardiac remodeling in infarcted rat hearts. *Ann Thorac Surg* 2008; 85: 562.
10. Iida H, Yokoyama I, Agostini D, et al. Quantitative assessment of regional myocardial blood flow using oxygen-15-labelled water and positron emission tomography: A multicentre evaluation in Japan. *Eur J Nucl Med* 2000; 27: 192.
11. Dib N, Michler RE, Pagani FD, et al. Safety and feasibility of autologous myoblast transplantation in patients with ischemic cardiomyopathy: Four-year follow-up. *Circulation* 2005; 112: 1748.
12. Perin EC, Dohmann HF, Borojevic R, et al. Transendocardial, autologous bone marrow cell transplantation for severe, chronic ischemic heart failure. *Circulation* 2003; 107: 2294.
13. Leor J, Aboulafia-Etzion S, Dar A, et al. Bioengineered cardiac grafts. A new approach to repair the infarcted myocardium? *Circulation* 2000; 102(suppl III): III-56.

14. Li RK, Jia ZQ, Weisel RD, et al. Survival and function of bioengineered cardiac grafts. *Circulation* 1999; 100(suppl II): II-63.
15. Suzuki K, Murtuza B, Beauchamp JR, et al. Role of interleukin-1beta in acute inflammation and graft death after cell transplantation to the heart. *Circulation* 2004; 110(11 suppl 1): II-219.
16. Tanaka H, Kawai H, Tatsumi K, et al. Relationship between regional and global left ventricular systolic and diastolic function in patients with coronary artery disease assessed by strain rate imaging. *Circ J* 2007; 71: 517.
17. Tanaka H, Kawai H, Tatsumi K, et al. Improved regional myocardial diastolic function assessed by strain rate imaging in patients with coronary artery disease undergoing percutaneous coronary intervention. *J Am Soc Echocardiogr* 2006; 19: 756.
18. Moller JE, Hillis GS, Oh JK, et al. Wall motion score index and ejection fraction for risk stratification after acute myocardial infarction. *Am Heart J* 2006; 151: 419.
19. Liu Y, Rajur K, Tolbert E, et al. Endogenous hepatocyte growth factor ameliorates chronic renal injury by activating matrix degradation pathways. *Kidney Int* 2000; 58: 2028.
20. Miyagawa S, Sawa Y, Taketani S, et al. Myocardial regeneration therapy for heart failure: Hepatocyte growth factor enhances the effect of cellular cardiomyoplasty. *Circulation* 2002; 105: 2556.
21. Taniyama Y, Morishita R, Aoki M, et al. Therapeutic angiogenesis induced by human hepatocyte growth factor gene in rat and rabbit hindlimb ischemia models: Preclinical study for treatment of peripheral arterial disease. *Gene Ther* 2001; 8: 181.
22. Li Q, Li B, Wang X, et al. Overexpression of insulin-like growth factor-1 in mice protects from myocyte death after infarction, attenuating ventricular dilation, wall stress, and cardiac hypertrophy. *J Clin Invest* 1997; 100: 1991.
23. Bock-Marquette I, Saxena A, White MD, et al. Thymosin beta4 activates integrin-linked kinase and promotes cardiac cell migration, survival and cardiac repair. *Nature* 2004; 432: 466.

TISSUE ENGINEERING: Part C
Volume 16, Number 3, 2010

DOI: 10.1089/ten.tec.2009.0362

Cardiomyoblast-like Cells Differentiated from Human Adipose Tissue-Derived Mesenchymal Stem Cells Improve Left Ventricular Dysfunction and Survival in a Rat Myocardial Infarction Model

Hanayuki Okura, M.S.,[1–4] Akifumi Matsuyama, M.D., Ph.D.,[1] Chun-Man Lee, M.D., Ph.D.,[1,2] Ayami Saga, M.S.,[1] Aya Kakuta-Yamamoto, B.S.,[1] Anna Nagao, B.S.,[1,2] Nagako Sougawa, D.M.D., Ph.D.,[1] Naosumi Sekiya, M.D.,[3] Kazuhiro Takekita, M.S.,[1,2] Yashuhiro Shudo, M.D.,[3] Shigeru Miyagawa, M.D., Ph.D.,[3] Hiroshi Komoda, M.D., Ph.D.,[1,5] Teruo Okano, Ph.D.,[6] and Yoshiki Sawa, M.D., Ph.D.[2,3]

Adipose tissue–derived mesenchymal stem cells (ADMSCs) are multipotent cells. Here we examined whether human ADMSCs (hADMSCs) could differentiate into cardiomyoblast-like cells (CLCs) by induction with dimethylsulfoxide and whether the cells would be utilized to treat cardiac dysfunction. Dimethylsulfoxide induced the expression of various cardiac markers in hADMSCs, such as α-cardiac actin, cardiac myosin light chain, and myosin heavy chain; none of which were detected in noncommitted hADMSCs. The induced cells were thus designated as hADMSC-derived CLCs (hCLCs). To confirm their beneficial effect on cardiac function, hCLC patches were transplanted onto the Nude rat myocardial infarction model, and compared with noncommitted hADMSC patch transplants and sham operations. Echocardiography demonstrated significant short-term improvement of cardiac function in both the patch-transplanted groups. However, long-term follow-up showed rescue and maintenance of cardiac function in the hCLC patch-transplanted group only, but not in the noncommitted hADMSC patch-transplanted animals. The hCLCs, but not the hADMSCs, engrafted into the scarred myocardium and differentiated into human cardiac troponin I-positive cells, and thus regarded as cardiomyocytes. Transplantation of the hCLC patches also resulted in recovery of cardiac function and improvement of long-term survival rate. Thus, transplantation of hCLC patches is a potentially effective therapeutic strategy for future cardiac tissue regeneration.

Introduction

END-STAGE HEART FAILURE remains a major cause of death worldwide, with most cases due to ischemia. This is despite the remarkable progress in recent years in both medical and surgical treatments for heart failure. Cardiac transplantation and mechanical support using implantation of the left ventricular assist system were established as the ultimate means of support for these patients.[1,2] However, these treatment entities have limitations including donor shortage, rejection, and left ventricular assist system durability, and alternative strategies are needed in such circumstances.

Cellular cardiomyoplasty was developed as a new approach to restore impaired heart function,[3,4] using a variety of cell types, with encouraging initial results.[3–5] Mesenchymal stem cells (MSCs) seem particularly advantageous for cellular therapy in general because they are multipotent, potentially immune privileged,[6] and expand easily *ex vivo*. MSCs also proliferate rapidly, induce angiogenesis, and can differentiate into cardiomyogenic cells.[7–10] An MSC population was recently isolated from human adipose tissue, which is abundantly available and can be resected easily and safely in most patients.[11,12] These adipose tissue-derived cell lineages showed cardiomyocytic differentiation and rescued

[1]Department of Somatic Stem Cell Therapy, Foundation for Biomedical Research and Innovation, Kobe, Japan.
[2]Medical Center for Translational Research, Osaka University Hospital, Suita, Japan.
[3]Department of Surgery, Osaka University Graduate School of Medicine, Suita, Japan.
[4]Research Fellow of the Japan Society for the Promotion of Science, Tokyo, Japan.
[5]Department of Internal Medicine, National Hospital Organization Chiba Medical Center, Chiba, Japan.
[6]Institute of Advanced Biomedical Engineering and Science, Tokyo Women's Medical University, Tokyo, Japan.

cardiac dysfunction in a myocardial infarction (MI) animal model. Thus, the adipose tissue is a convenient and preferred source of stem cell recovery for cardiac therapy. Recently, transplantation of monolayered adipose tissue-derived MSCs (ADMSCs) into MI rats reversed wall thinning in the scarred area and improved cardiac function in a short term, with the engrafted sheet of cells forming a thick stratum containing newly formed vessels and scattered cardiomyocytes derived from the implanted cells.[13] As patients with severe heart failure desire sustained and long-term recovery of cardiac function after treatment rather than short-term improvement, continued efforts should be made to develop cell transplants from ADMSCs that survive and differentiate into cardiomyocytes *in vivo* for subsequent engraftment onto scarred myocardium.

This study investigated the differentiation of human ADMSCs (hADMSCs) into cardiomyoblast-like cells (CLCs) *in vitro*, analyzed the functional and histological regeneration of damaged myocardium after transplantation of CLCs *in vivo*, and examined the effects of such transplantation on long-term patient survival.

Materials and Methods

Adipose tissues from human subjects

Excess omental adipose tissues were resected from the gastro-omental artery during coronary artery bypass graft surgery and gastrectomy in 10 subjects [4 men and 6 women; age, 55 ± 5 years, mean ± standard error of mean (SEM); range, 40–60 years]. All subjects provided informed consent, and the Review Board for Human Research of Osaka University Graduate School of Medicine approved all protocols. All subjects fasted for at least 10 h before surgery and none was on steroid therapy at the time of surgery. Ten to 50 grams of adipose tissue was obtained from each subject.

Isolation of hADMSCs and differentiation into CLCs

hADMSCs were obtained as reported previously, with modification.[11,14] Briefly, the resected excess adipose tissue was minced and then digested at 37°C for 1 h in Hank's balanced salt solution (Gibco–Invitrogen, Grand Island, NY) containing 0.075% collagenase type II (Sigma–Aldrich, St. Louis, MO). Digests were filtered through a cell strainer (BD Bioscience, San Jose, CA) and centrifuged at 800 *g* for 10 min. Red blood cells were excluded using density gradient centrifugation with Lymphoprep ($d = 1.077$; Nycomed, Oslo, Norway), and the remaining cells were cultured in Dulbecco's modified Eagle's medium (Gibco–Invitrogen) with 10% defined fetal bovine serum (Hyclone, Logan, UT) for 24 h at 37°C. Following incubation, the adherent cells were washed extensively and then treated with 0.2 g/L ethylenediaminetetraacetate solution (Nacalai Tesque, Kyoto, Japan). The resulting suspended cells were replated at a density of 10,000 cells/cm^2 on human fibronectin-coated dishes (BD BioCoat, Franklin Lakes, NJ) in 60% Dulbecco's modified Eagle's medium-low glucose, 40% MCDB-201 medium (Sigma–Aldrich), 1 × insulin-transferring selenium (Gibco–Invitrogen), 1 nM dexamethasone (Sigma–Aldrich), 100 μM ascorbic acid 2-phosphate (Sigma–Aldrich), 10 ng/mL epidermal growth factor (PeproTec, Rocky Hill, NJ), and 5% fetal bovine serum. After passaging five to six times in the same medium, the hADMSCs were used for transplantation. Cardiomyocytic differentiation was achieved by inducing hADMSCs with 0.1% dimethylsulfoxide (DMSO) for 48 h, resulting in a population named CLCs.

Reverse transcriptase–polymerase chain reaction

Total RNA was isolated from hADMSCs and cardiomyoblasts using an RNAeasy kit (Qiagen, Hilden, Germany). As a control, excess human myocardium was resected during maze surgery from 10 matched subjects (4 men and 6 women; age, 55 ± 5 years, mean ± SEM; range, 40–60 years) with informed consent. Control subjects also fasted for at least 10 h before surgery, and none was taking steroids. Approximately 1 g of myocardium was obtained from each subject, and the same protocol was performed to obtain total RNA. After treatment with DNase, cDNA was synthesized from 500 ng total RNA using Superscript III reverse transcriptase RNase H minus (Invitrogen, Carlsbad, CA). The absence of DNA contamination in RNA samples was confirmed with polymerase chain reaction (PCR) primers flanking an intron. Primers and the reaction conditions are described in Table 1. The PCR products were fractionated by 2% agarose gel electrophoresis.

Table 1. Primers Used in Reverse Transcriptase–Polymerase Chain Reaction

Primer		*Sequence*	*No. of cycles*	*Annealing temperature (°C)*
GAPDH	Forward	GTCAGTGGTGGACCTGACCT	35	60
	Reverse	AGGGGAGATTCAGTGTGGTG		
Islet-1	Forward	TGATGAAGCAACTCCAGCAG	35	60
	Reverse	GGACTGGCTACCATGCTGTT		
Nkx2.5	Forward	GGTGGAGCTGGAGAAGACAGA	35	60
	Reverse	CGACGCCGAAGTTCACGAAGT		
GATA-4	Forward	ACCAGCAGCAGCGAGGAGAT	35	60
	Reverse	GAGAGATGCAGTGTGCTCGT		
α-Cardiac actin	Forward	GGAGTTATGGTGGGTATGGGTC	35	60
	Reverse	AGTGGTGACAAAGGAGTAGCCA		
Myosin light chain-2v	Forward	5′-GCGCCAACTCCAACGTGTTCT	35	60
	Reverse	5′-GTGATGATGTGCACCAGGTTC		
Myosin heavy chain	Forward	GGGGACAGTGGTAAAAGCAA	35	60
	Reverse	TCCCTGCGTTCCACTATCTT		

Model animals for MI

The left anterior descending coronary artery of rats with severe combined immunodeficiency was ligated. In brief, rats were anesthetized with nembutal (40 mg/kg), before being intubated and ventilated at a rate of 60 cycles/min with a tidal volume of 5 mL under room air supplemented with oxygen (2 L/min). The hearts were exposed through the fifth left-intercostal space and the left anterior descending was ligated. After 4 weeks, the hearts were again exposed through the fifth left-intercostal space, and the infarct area was identified visually based on surface scarring and abnormal wall motion. Cell sheets were subsequently implanted onto the infarcted myocardium. The control group was treated similarly, but no cell sheets were implanted. The Osaka University Graduate School of Medicine Standing Committee on Animals approved all experimental protocols.

Preparation of monolayered cell sheets

After four to five passages, the hADMSCs were trypsinized and then replated onto 35-mm temperature-responsive dishes (CellSeed, Tokyo, Japan) in 2 mL of expansion medium at 1×10^6 cells per dish. After culture at 37°C for 2 days, 0.1% DMSO was added to the medium on half of the dishes to differentiate the hADMSCs into cardiomyoblasts. After 2 days of culture, the cells were incubated again at 20°C. Within 20 min, the hADMSCs and CLC sheets detached spontaneously and floated up into the medium for use as monolayered cell grafts.[13,15–17]

Assessment of rat cardiac function

Cardiac ultrasound studies were performed before ligation, before implantation, and at 2, 4, 8, 10, 12, 14, and 16 weeks after implantation using a SONOS 7500 (Philips Medical Systems, Andover, MA). Plasma atrial natriuretic protein (ANP) level was analyzed using an ANP ELISA system (Phoenix Pharmaceuticals, Burlingame, CA) by following the instructions supplied by the manufacturer.

Histological analyses

The rat hearts were dissected out and immediately fixed overnight in 4% paraformaldehyde, washed in 70% alcohol, dehydrated through a graded ethanol series, cleared in xylene, and finally processed for embedding in paraffin wax. Paraffin sections were cut at 5 μm thickness, delineated on the microscope slide using a Dako pen (Dako, Glostrup, Denmark), deparaffinized in xylene, and then rehydrated through a graded ethanol series into distilled water. The sections were then immersed in Target Retrieval Solution (Dako) in distilled water and boiled, followed by cooling at room temperature for 20 min. The sections were then washed in two changes of Tris-buffered saline (TBS), pH 7.4, followed by 1% polyoxyethylene sorbitan monolaurate (Tween 20) in TBS (TBS-T), and then an overnight incubation with 10% Blocking One® (Nacalai Tesque) in TBS-T. The sections were then incubated in a humid chamber for 16 h at 4°C with mouse monoclonal antibodies to α-cardiac actin (α-CA) and human troponin I, diluted in the blocking solution, followed by Alexa Fluor 546-labeled donkey anti-goat IgG (Molecular Probes, Eugene, OR). The stained slides were viewed on a BioZero laser scanning microscope (Keyence, Osaka, Japan).

Statistical analysis

All data were expressed as mean ± SEM. Differences between groups were analyzed for statistical significance by the Student's *t*-test using SPSS Statistics 17.0 (SPSS, Inc., Chicago, IL). A *p*-value less than 0.05 denoted a statistically significant difference. Survival curves were constructed by the Kaplan–Meier method and survival among groups was compared using the Log-Rank test (StatMate III for Windows; Atoms, Tokyo, Japan).

Results

Cardiac differentiation of hADMSCs into CLCs

The potential for hADMSCs to differentiate into CLCs was evaluated from the mRNA expression of several cardiac differentiation markers by reverse transcriptase-PCR before and after DMSO induction, as follows: *islet-1* is a cardiac stem cell marker; *Nkx2.5* and *GATA-4* are transcription factors required for subsequent cardiac differentiation; and α-*CA*, *myosin light chain*, and *myosin heavy chain* (*MHC*) are markers of cardiac differentiation (Fig. 1A). Preinduced hADMSCs expressed *islet-1* and *Nkx2.5* mRNA, but not that of *GATA-4*, α-*CA*, *myosin light chain*, or *MHC*. After induction by DMSO for 48 h, hADMSCs expressed all markers, indicating that DMSO treatment successfully differentiated hADMSCs into cells of the cardiac lineage, and these induced cells were named CLCs.

Preparation and transplantation of hADMSC-derived CLC patches

To evaluate the potential therapeutic usefulness of CLCs, we designed an experimental rat model of coronary ligated infarction to assess cardiac function after transplantation of CLC patches. CLC and control hADMSC patches were prepared from cell sheets, as described earlier (Fig. 1B). These patches were transplanted onto the scarred area of the left ventricular wall in the MI model Nude rats, whose left anterior descending artery had been ligated 4 weeks before graft implantation (Fig. 1C, D). Sham transplantations were also performed.

Effects of CLC transplantation on cardiac function and survival rate

Cardiac function was assessed by echocardiography at preligation, pretransplantation, and every 2 weeks after transplantation (Fig. 1D). Sixteen weeks after transplantation, the treated animals were sacrificed and cardiac tissues prepared for histological examination. Four weeks after graft implantation, wall motion was improved in both control and CLC patch-implanted hearts. However, the wall motion of control and noncommitted hADMSC patch-transplanted heart tissue was exacerbated at 16 weeks after transplantation, while improved motion was maintained with the CLC patch transplants (Fig. 2A). In the early phases of the post-transplantation period, left ventricular diastolic dimension was significantly reduced in both the transplanted groups, but by 8 weeks after implantation this parameter increased in the control hADMSC patch-transplanted group, whereas it remained unchanged in those animals that received CLC patch transplants (Fig. 2B). Likewise, left ventricular ejection

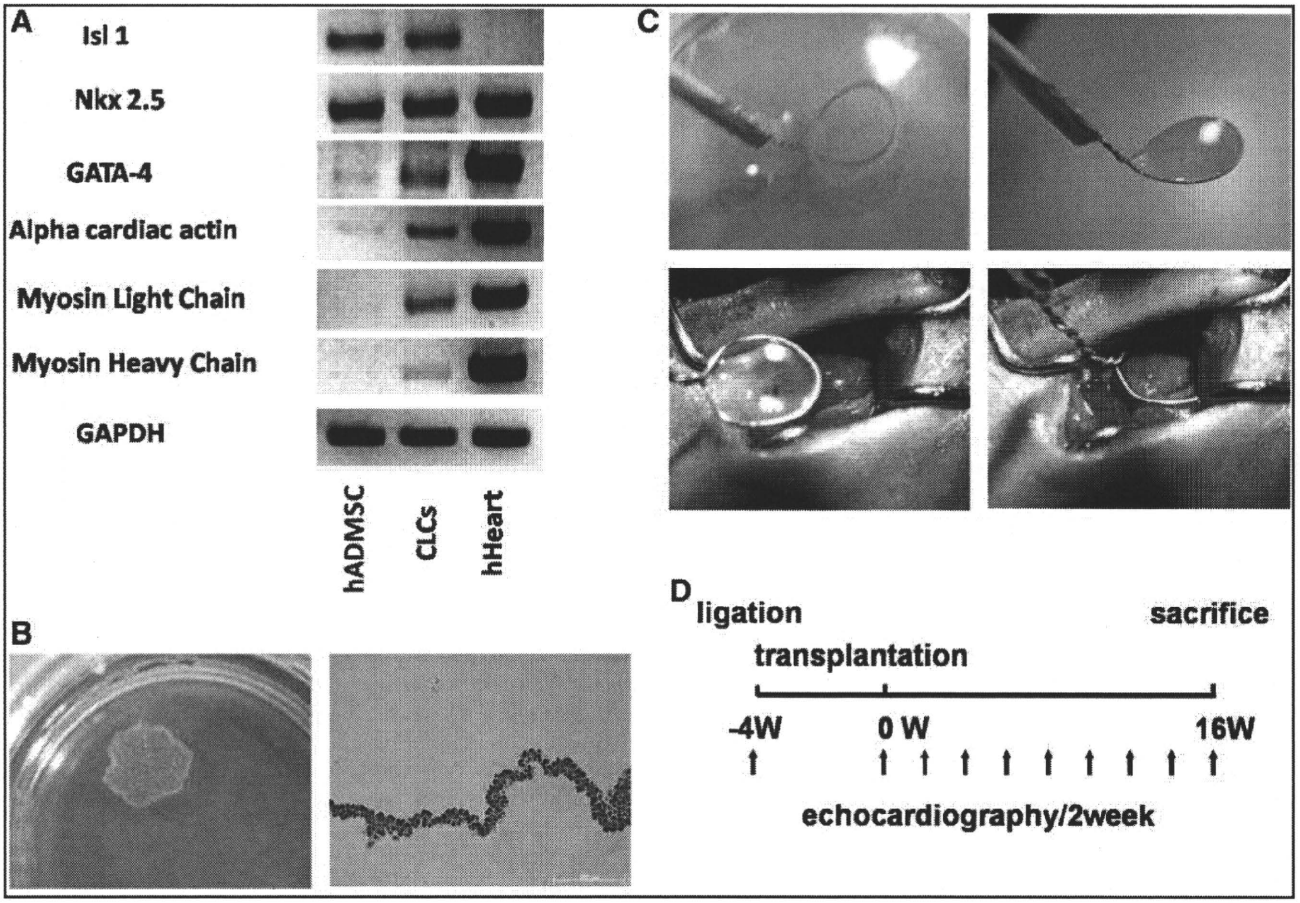

FIG. 1. Preparation and transplantation of human adipose tissue-derived mesenchymal stem cell (hADMSC)-derived cardiomyoblast-like cell (hCLC) patches. (**A**) Treatment with dimethylsulfoxide (DMSO) transformed hADMSCs into CLCs. The mRNA expressions of *islet-1*, *Nkx2.5*, *GATA-4*, *α-cardiac actin* (*α-CA*), *myosin light chain* (*MLC*), and *MHC* were analyzed by reverse transcriptase–polymerase chain reaction. The mRNAs for *islet-1* and *Nkx2.5*, with trace levels of *GATA-4* and *α-CA*, were expressed in hADMSCs, but no expression of *MLC* or *MHC* was detected. After induction with DMSO for 48 h, the hADMSCs also expressed *MLC* and *MHC*, indicating a phenotypic change into CLCs. (**B**) Preparation of hADMSC-derived CLC patches. The hADMSCs were cultured on temperature-responsive dishes for 48 h with 0.1% of DMSO for differentiation into CLCs. As the culture temperature was decreased from 37°C to 20°C, the CLCs detached spontaneously as sheets and floated up within 30 min into the culture media as a layered CLC patch. (**C**) Transplantation of hADMSC-derived CLC patches. Detached patches were transplanted onto the left ventricular wall scar in the myocardial infarction (MI) model Nude rats. (**D**) Protocol used for assessment of cardiac function. The left anterior descending artery was ligated in Nude rats at 4 weeks before graft implantation. Cardiac function was assessed by echocardiography at preligation, pretransplantation, and every 2 weeks following transplantation. The treated animals were sacrificed 16 weeks after transplantation and prepared for histological examination.

fractions improved in both the implanted groups until 8 weeks, after which time it worsened only in the group transplanted with noncommitted hADMSC patches (Fig. 2B).

ANP was then measured to confirm that chronic heart failure due to MI could be treated by CLC patch transplantation (Fig. 2C). The ANP levels were significantly increased after MI in all groups (Fig. 2C). The sham-operated MI control group showed incremental increases in plasma ANP over the time course of examination, whereas both CLC patch- and hADMSC patch-transplanted animals had low ANP levels until 8 weeks after treatment. However, ANP levels increased subsequently in the hADMSC patch-transplanted group, whereas the CLC patch-transplanted group maintained the improvement in ANP levels.

The Kaplan–Meier survival curve showed higher long-term survival rates in cell patch-transplanted groups than in sham-operated MI controls (Fig. 2D). Notably, no rat died after transplantation of an hADMSC-derived CLC patch. Survival at 16 weeks after surgery was 100% for the CLC group, 80% for the hADMSC group, and 16% for the sham-operated group, with a significant difference between the two transplanted groups. These results suggest that transplantation of hADMSC-derived CLCs has beneficial effect in rats with heart failure induced by MI.

Effects of CLC transplantation on cardiac structure

Cardiac structure was next examined histologically to analyze further the difference between CLC patch- and noncommitted hADMSC patch-transplanted animals in the longer term (Fig. 3). On hematoxylin and eosin and Masson trichrome staining, the sham-transplanted MI control rats

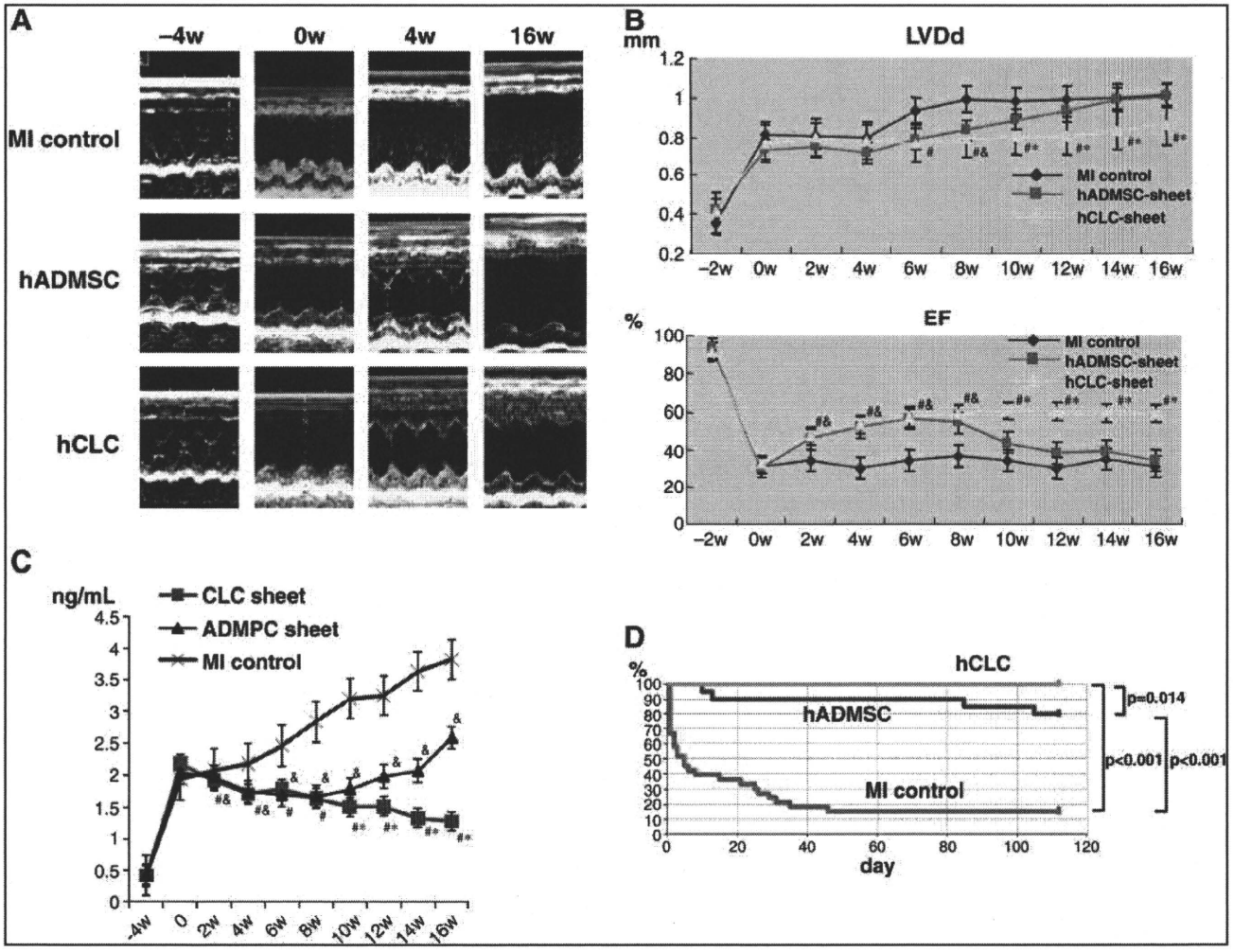

FIG. 2. Effects of CLC patch transplantation on cardiac function and long-term survival. (**A**) In both the patch-transplanted groups, echocardiography showed improved wall motion within 4 weeks of transplantation. However, at 16 weeks after transplantation, the wall motion of noncommitted hADMSC patch-transplanted rats worsened, whereas it was maintained in the CLC patch-transplanted animals. (**B**) Left ventricular diastolic dimension and ejection fractions improved significantly in both the patch-grafted groups in the early phase, as confirmed by echocardiography. However, these two parameters of cardiac function worsened at 8 weeks after implantation in the noncommitted hADMSC patch-transplanted groups, but not in the CLC patch-transplanted group. The numbers of all groups were five. Data are mean ± standard error of mean ($^{\#}p < 0.05$; MI control vs. the hCLC patch-transplanted animals; $^{\&}p < 0.05$; MI control vs. the noncommitted-hADMSC patch-transplanted rats; $^{*}p < 0.05$; hCLC patch-transplanted vs. the noncommitted hADMSC patch-transplanted rats, respectively). (**C**) Plasma ANP levels. Sham-operated MI control group showed increment of plasma ANP levels during the course of the experiment. Both the CLC patch- and hADMSC patch-transplanted groups showed suppression of ANP level increment till 8 weeks after treatment. ANP levels of the hADMSC patch-transplanted group increased from 8 weeks after transplantation, but no change in ANP levels was noted in the CLC patch-transplanted group. The numbers of all groups were four. (**D**) Long-term survival of rats with chronic heart failure that received the CLC patch ($n = 28$), noncommitted hADMSC patch ($n = 20$), or sham operation ($n = 37$). The Kaplan–Meier survival curve demonstrated that no rat died after transplantation of hADMSC-derived CLC patch. The survival rate at 16 weeks after surgery was 80% for the hADMSC group versus 16% for the sham-operated group. Log-rank test; p-values are indicated. LVDd, left ventricular diastolic dimension.

showed only a thin layer of cardiac muscle and fibrotic tissues in the scarred anterior left ventricular wall (Fig. 3A, B). Rats implanted with noncommitted hADMSCs showed small patches of cardiac muscles over that seen in the control MI rats (Fig. 3C, D). On the other hand, the rats transplanted with CLC patches showed significant reversal of the infracted myocardium and a full cardiac muscle layer overlaying the transplanted area (Fig. 3E, F, arrowheads).

CLCs differentiate into cardiac muscle in situ

The *in situ* differentiation capacity of the implanted cell sheets into cardiomyocytes after grafting onto the scarred myocardium was assessed by immunohistochemical staining for α-CA and human troponin I (Fig. 4). Thin layers of α-CA-positive cells were observed on the scarred myocardium of sham-operated MI control rats (Fig. 4A). A similar but thicker